energyequipsys/Vol1/ 2013/ 35-58

ENERGY EQUIPSYS

Energy Equipment and Systems
www.energyequipsys.com

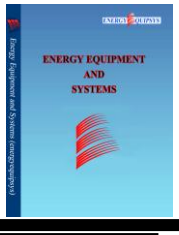

Drag coefficient and strouhal number analysis of cylindrical tube in two phase flow

Pedram Hanafizadeh [a*]
Sina Karbalaee M.
Behdad Sharbaf E.
S. Ghanbarzadeh [b]

[a] Center of Excellence in Design and Optimization of Energy Systems, School of Mechanical Engineering, College of Engineering, University of Tehran, P.O. Box 11155-4563, Tehran, Iran

[b] School of Petroleum Engineering, Texas University at Austin, Austin, Texas, USA

Article history:

Received 25 May 2013
Accepted 18 June 2013

ABSTRACT

In many industrial equipment such as boilers and heat exchangers, the cylindrical tubes are exposed to the gas- liquid two phase flow. For any immersed body in flow field vortex shedding is created with a frequency that may be constant or variable, according to conditions such as flow rates, geometry of body, and etc. The failure will happen in the equipment, when this frequency is close to one of the natural frequencies of them. This can cause noise and flow induced vibration problem which is one of the main defects in the heat exchangers. Therefore considering these flows can play a significant role in long-term reliability and safety of industrial and laboratory equipment. In this study Eulerian–Eulerian approach is employed to simulate two-phase flow around the cylindrical tube. Since the Reynolds Stress Model (RSM) accounts for the effects of streamline curvature, swirl, rotation, and rapid changes in strain rate in a more rigorous manner than other turbulence models, it has greater potential to give accurate predictions for complex flows. So in this study the RSM is used to recognize behavior of vortex shedding in the flow. Drag coefficient, Strouhal number, vortex shedding behind cylinder, void fraction and pressure coefficient distribution were investigated in air-water two phase flows. In order to verify validity of CFD model, inlet void fraction was set to zero, Strouhal number and it's relation with low Reynolds number (100-3000) in single phase flow were compared with experimental and numerical result of available literatures. The results show a good agreement between them. Having reasonable judgment of fluctuating lift force frequency, fast Fourier transform (FFT) was applied to lift coefficient of cylinder. The FFT produces averaged spectral coefficients that are independent of time and are useful to identify dominant frequencies in a signal. Some remedies were introduced to reduce vortex frequency of cylindrical tube subjected in gas-liquid two phase flows and protect tube from hard vibrations. For this purpose, some geometrical modifications were applied and results showed that in all cases drag coefficient and Strouhal number reduce.

Keywords: Fast Fourier Transform, Flow Induced Vibration, Reynolds Stress Model, Strouhal Number, Two Phase Flow, Vortex Frequency.

1. Introduction

Gas- liquid two phase flow occurs in a wide range of natural and man-made situations such as boiling heat transfer, cloud cavitations, bubble columns and reactors in the chemical industry, cooling circuits of power plants, spraying of liquid fuel and paint, rain, bubbles and drops due to wave breaking in the oceans, and explosive volcanic eruptions. Also, two-phase cross flow over tubes occurs in many shell-and-tube heat exchangers, steam generators, condensers and other equipment utilized in power and process industries, so it is very important for a plant to estimate pressure loss of flow in various conduits. A reduction of the pressure drop results in an improvement of the total plant efficiency. In many flow systems, complex conduits with flow obstacles have been widely employed and the flow in them is often gas-liquid two phase. However, only a few studies of the two-phase drag experienced by such tubes have been reported in the literature, because of its complexity and heterogeneity. Knowledge of the drag coefficient for a tube, the void fraction distribution and bubble behavior near a tube subjected to two-phase cross flow is essential for development of mechanistic understanding of fluid elastic instability of tubes subjected to two-phase cross flow.

1.1. Experimental Works

Yokosawa et al. [1] measured the drag on a single tube under two-phase cross flow in the Reynolds number

*Corresponding author:
Center of Excellence in Design and Optimization of Energy Systems, School of Mechanical Engineering, College of Engineering, University of Tehran, P.O. Box 11155-4563, Tehran, Iran
E-mail address: hanafizadeh@ut.ac.ir, (Pedram Hanafizadeh)

range of 4000-300,000 and for low void fractions (0-0.1). They found that the drag coefficient decreased with increasing void fraction for two-phase Reynolds numbers sufficiently below the single-phase critical Reynolds number. But, for Reynolds numbers above the critical value, the drag coefficient gradually increased with increasing void fraction, although it remained significantly less than the value for subcritical, single-phase flow. They also classified flow patterns of the two-phase wake flow behind a cylinder and investigated quantitatively the change of the drag coefficient corresponding to the transition of the flow patterns. In the first part of another study by Inoue et al. [2], the void fraction distribution around the tube was measured with an electrical impedance probe inserted in the flow in the Reynolds number range of 5000-80,000. They found that high void fraction regions, with the local void fraction about 3-4 times higher than the free stream value, were produced near the separation point. As the mean velocity in the main flow increased, this peak void fraction also increased and the location of the peak void fraction came closer to the cylinder. They also carried on some experiments to clarify the two-phase flow and heat transfer characteristics around a body including the unknown complicated flow behavior. In their report, the flow characteristics near and behind a cylinder which was located in a vertical upward air-water bubbly flow were investigated. From the observation of the flow patterns and the measurements of the distribution of void fraction, liquid velocity and static pressure, it is revealed that the vortex flow and the change of the static pressure and liquid velocity distribution around the cylinder resulted in the large distortion of the void fraction distribution around the cylinder. The most important note in their work was the phenomena in the wake that the peaks of the local void fraction appeared in the vicinity of the cylinder surface near the separation point and in the wake behind the cylinder. Pettigrew et al. [3] studied vibrations of a tube in a square array, in a normal triangular array and in a parallel triangular array configuration. By taking photographs of the flow at the end of the bundle, they observed relatively stagnant zones of mostly liquid immediately upstream and downstream of each tube. Joo and Dhir [4] did some experiments to investigate drag coefficient based on pressure distribution on cylinder. In their experiments, liquid Reynolds number ranged from 430 to 21,900 for the single tube and liquid gap Reynolds number ranged from 32,900 and 61,600 for the tube placed in a triangular array. Free stream void fraction was varied from 0 to 0.4. At low Reynolds numbers, the ratio of two-phase to single-phase drag coefficient is found to be a strong function of Gr/Re^2. However, at high Reynolds numbers only void fraction is the important parameter. Empirical correlations have been developed for the ratio of two-phase drag on a single tube and on a tube placed in an array. Other reports which we have been able to find were Hara & Ohtani [5, 6] and Hulin et al. [7].The former discussed the fluctuation characteristics in surface pressure, lift and drag forces on a cylinder in the two-phase cross flow. The latter reported the vortex emission behind a trapezoidal cylinder. A series of our studies, therefore, are intended to clarify the two-phase flow characteristics around a body, which include the unknown complicated flow behavior.

1.2. Numerical Works

Among the whole variety of numerical simulation studies of two-phase flows, some works deserve mention. For the most part, these studies addressed the case of upward flow of two-phase gas–liquid systems. But Artemiev and Kornienko [8] and Zaichik et al. [9] reported some results for downward gas–liquid flows.

A numerical model predicting how the shape of void fraction profiles affects the distribution of temperature and liquid-phase velocity in vertical flows was developed by Artemiev and Kornienko [8]. This model can be applied both to upward and downward flows. In their work, enhanced turbulence due to gas bubbles present in the flow was taken into account. The turbulent viscosity was represented as a linear combination of two terms, one term being due to the liquid-phase turbulence, which can be calculated by the Reichardt formula, and the other term modeling the additional viscosity due to the relative gas motion. The second term involves some empirical constants, this circumstance making the developed numerical model less general. In works done by Zaichik et al. [9], a diffusion-inertia model for the transport of low-inertia particles of arbitrary density was proposed. The predicted data were compared with the experimental data of Kamp et al. [10] for gas–liquid flows in vertical pipes (the cases of downward and upward flow under various conditions of the effect due to the gravity force). It was shown possible, in principle, to analyze bubbly flows with the help of the diffusion-inertia model, initially developed for gas-dispersed flows. To calculate the liquid turbulence, the $k-\epsilon$ model of turbulence for single--phase flow was used.

Antal et al. [11] developed a numerical model for transport phenomena in laminar upward bubbly flow. The model was based on the Eulerian two-velocity approach. The major forces acting on bubbles in the laminar flow were the lifting (Saffman) force and the wall force. In Lopez et al. [12] works, a numerical and experimental study of turbulent bubbly flow in a triangular channel was reported. By Carrica et al. [13] and Palitano et al. [14], the case of poly-dispersed two-phase flows was addressed. The model makes it possible to allow for the shift of the bubble concentration maximum from the near-wall zone towards the flow core observed when the dispersed-phase size increases above some critical values. Troshko and Hassan [15] developed a numerical model involving the law of the wall for vertical mono-dispersed bubbly flow in a pipe.

In Lopez et al. [12], Carrica et al. [13], Palitano et al. [14], Troshko and Hassan [15] and Lee et al. [16] to predict the liquid-phase turbulence, a two-equation

model of turbulence extended to the case of two-phase flow, was used. It can be stated that, in spite of the intensive recent efforts aimed at numerical investigation of downward gas–liquid flows, gained data cover only a narrow range of parameters and therefore apply only to particular conditions.

Ghanbarzadeh et al. [17] used a numerical approach to predict the drag coefficient and void fraction around a cylindrical probe. They also used an image processing technique to demonstrate the distribution of void fraction around different cross-section prisms.

The purpose of the present study is a numerical investigation of the structure of cross gas–liquid flow over some selected bodies. A model constructed around the Eulerian representation for both phases was developed to numerically examine the structure of flow field and wake zone behind cylinders in mono-dispersed gas–liquid flow.

A numerical study of flow characteristics around a cylinder which was located in a uniform air-water bubbly flow is performed to achieve better understanding of the fundamental flow aspects. Since local flow direction changes around a body, two-phase cross flow is affected significantly by fluid inertia. Therefore, the quite different flow behavior between gas and liquid is induced, because of large density difference between phases. Consequently, the void fraction distribution around the body changes remarkably.

Afterward, some geometrical modifications subject to two-phase cross-flow is investigated, in addition to a conventional cylinder. For detecting and considering flow characteristic around these objects same numerical algorithm were applied and the results were discussed in next parts.

In a gas-liquid bubbly flow, there exists more intensive turbulence, as compared with the single-phase flow, due to the disturbance induced by the bubbles. Moreover, since there appears large difference in the behaviors of both phases induced by the gradient of static pressure near the cylinder surface, the intensive turbulence is generated there. Momentum transported from the main flow to the boundary layer becomes fairly large in the two-phase flow. Therefore, large reduction in the transition Reynolds number seems to be realized in the two-phase cross flow. Consequently, total pressure loss of the two-phase flow can be reduced in such complex conduits with flow obstacles, as flow around rod spacers in a fuel assembly and flow across a cluster of pipes in a steam generator. The characteristics of the unsteady motion in the two-phase flow which may closely relate to the strong turbulence and the bubble behavior are also important research subjects in a series of our studies. In the present article, the fundamental characteristics of the two-phase wake flow around a cylinder have been investigated in order to answer the various complicated questions as mentioned above. At present no quantitative and enough correlations for two-phase Strouhal number, drag and pressure coefficients on cylinders subjected to two-phase cross flow are available in the literatures. The purpose of this numerical work is to consider such characteristics in gas- liquid two phase flow around the cylinder. At other part of this study some geometrical modifications were applied to the cylinder to modify the Strouhal number. Also numerical simulation was performed to investigate flow field around and especially behind the cylinders and find the optimum modified geometry in an air-water two-phase flow. Finally the optimized geometry was considered to find drag, lift and pressure coefficients for different two phases Reynolds numbers and various air inlet volume fractions.

2. Numerical Approach

2.1. Eulerian-Eulerian Model

In the Euler-Euler approach [18-22], the different phases are treated mathematically as interpenetrating continua. Since the volume of a phase cannot be occupied by the other phases, the concept of phasic volume fraction is introduced. These volume fractions are assumed to be continuous functions of space and time and their sum is equal to one. Conservation equations for each phase are derived to obtain a set of equations, which have similar structure for all phases. These equations are closed by providing constitutive relations that are obtained from empirical information or in the case of granular flows, by application of kinetic theory.

The Eulerian model is the most complex of the multiphase flow numerical models. It solves a set of n momentum and continuity equations for each phase. Coupling is achieved through the pressure and interphase exchange coefficients. The manner in which this coupling is handled depends upon the type of phases involved; granular (fluid-solid) flows are handled differently than non-granular (fluid-fluid) flows. For granular flows, the properties are obtained from application of kinetic theory. Momentum exchange between the phases is also dependent upon the type of mixture being modeled. Applications of the Eulerian multiphase model include bubble columns, risers, particle suspension, and fluidized beds.

2.1.1.Volume Fractions

The description of multiphase flow as interpenetrating continua incorporates the concept of phasic volume fractions, denoted here by α_q. Volume fractions represent the space occupied by each phase, and the laws of conservation of mass and momentum are satisfied by each phase individually. The derivation of the conservation equations can be done by ensemble averaging the local instantaneous balance for each of the phases [23] or by using the mixture theory approach [24].

The volume of phase q (V_q), is defined by:

$$V_q = \int_V \alpha_q \, dV \tag{1}$$

where

$$\sum_{q=1}^{n} \alpha_q = 1 \tag{2}$$

The effective density of phase q is:

$$\hat{\rho}_q = \alpha_q \rho_q \tag{3}$$

2.1.2.Conservation of Mass

The continuity phase averaged equation for phase q is:

$$\frac{\partial}{\partial t}(\bar{\alpha}_q \rho_q) + \nabla.(\bar{\alpha}_q \rho_q \tilde{V}_q) = 0 \tag{4}$$

2.1.3.Conservation of Momentum

Neglecting laminar stress- strain tensor, gravity and other body forces, the momentum balance for phase q yields:

$$\frac{\partial}{\partial t}(\bar{\alpha}_q \rho_q \tilde{V}_q) + \nabla.(\bar{\alpha}_q \rho_q \tilde{V}_q \otimes \tilde{V}_q) = -\bar{\alpha}_q \nabla \tilde{p} + \nabla.\tilde{\tau}_q^t + F_{pq} \tag{5}$$

The tilde indicates phase- averaged variables while an over bar reflects time- averaged values. For instance the phase average value of V for phase q, is defined by:

$$\tilde{V}_q = \frac{\overline{\alpha_q V_q}}{\overline{\alpha_q}} \tag{6}$$

In Eq.(5) F_{pq} is the drag force between the water and air phases and can be defined as:

$$F_{pq} = K_{pq}\left[(\tilde{V}_p - \tilde{V}_q) - \left(\frac{\overline{\alpha_p v'_p}}{\overline{\alpha_p}} - \frac{\overline{\alpha_q v'_q}}{\overline{\alpha_q}}\right)\right] \tag{7}$$

where K_{pq} is the drag coefficient is defined by Schiller-Nauman model [25]. Several terms in the above equations are required to be modeled to close the phase averaged momentum equations. More descriptions of all assumptions are available in Cokljat et al work [26].

2.1.4.Turbulence Model

The turbulent stresses $\nabla.\tilde{\tau}_q^t$ appeared in the momentum equations are defined on a per- phase basis and calculated as:

$$\tilde{\tau}_q^t = -\bar{\alpha}_q \rho_q \tilde{R}_{q,ij} \tag{8}$$

In above equations subscript q can be replaced by w for water phase or a for air phase. The present RSM multiphase model solves transport equations for the Reynolds stresses $\tilde{R}_{ij}$. As the concentration of air phase is dilute in the water phase, the dispersed turbulence model is used here. Therefore the water phase turbulence is considered as the dominant turbulence potential. Consequently, the transport equations for turbulence quantities are only solved for the water phase and the turbulence quantities for air phase will be predicted by Tchen theory [27]. The transport equation for the water phase Reynolds stresses is:

$$\frac{\partial}{\partial t}(\bar{\alpha}\rho\bar{R}_{ij}) + \frac{\partial}{\partial x_q}(\bar{\alpha}\rho\vec{U}_q\bar{R}_{ij}) = -\bar{\alpha}\rho\left(\bar{R}_{iq}\frac{\partial \vec{U}_j}{\partial x_q} + \bar{R}_{jq}\frac{\partial \vec{U}_i}{\partial x_q}\right) + \frac{\partial}{\partial x_q}\left[\bar{\alpha}\mu\frac{\partial}{\partial x_q}(\bar{R}_{ij})\right] - \frac{\partial}{\partial x_q}\left[\bar{\alpha}\rho\overline{\acute{u}_i\acute{u}_j\acute{u}_k}\right] + \bar{\alpha}P\left(\frac{\partial \acute{u}_i}{\partial x_j} + \frac{\partial \acute{u}_j}{\partial x_i}\right) - \bar{\alpha}\rho\bar{\varepsilon}_{ij} + \Pi_{R,ij} \tag{9}$$

All variables for the transport equation are defined for water phase. The last term in the transport equation, $\Pi_{R,ij}$, presents the turbulence interaction between the water and air phases and will be modeled by:

$$\Pi_{R,ij} = K_{wa}\left[\frac{\overline{\acute{u}_{w,i}}(\bar{U}_{a,i} - \bar{U}_{w,i}) + \overline{\acute{u}_{w,i}}(\bar{U}_{a,j} - \bar{U}_{w,j})}{\acute{u}_{w,j}(\acute{u}_{a,i} - \acute{u}_{w,i}) + \acute{u}_{w,i}(\acute{u}_{a,j} - \acute{u}_{w,j})}\right] \tag{10}$$

To simplify this term neglecting the anisotropy of the exchange term and consider the following assumption:

$$\Pi_{R,ij} = \frac{2}{3}\delta_{i,j}\Pi_{pq} \tag{11}$$

where δ_{ij} is the Kronrcker delta and Π_q represents the modified version of the original Simonin model [28].

$$\Pi_{pq} = K_{pq}(\tilde{k}_{pq} - 2\tilde{k}_q + \tilde{V}_{rel}.\tilde{V}_{drift}) \tag{12}$$

where, $\tilde{k}_q$ shows the turbulent kinetic energy of the water phase, $\tilde{k}_{pq}$ represents the water- air phase velocity covariance, and $\tilde{V}_{rel}$ and $\tilde{V}_{drift}$ stand for the relative and drift velocities, respectively.

$$\tilde{k}_{pq} = 2\tilde{k}_q\left(\frac{b + \eta_{pq}}{1 + \eta_{pq}}\right)$$
$$\tilde{k}_p = 2\tilde{k}_q\left(\frac{b^2 + \eta_{pq}}{1 + \eta_{pq}}\right)$$
$$v_d^t = \frac{1}{3}\tilde{k}_{pq}\tau_{pq}^t + \left(\frac{2}{3}\tilde{k}_p - b\frac{1}{3}\tilde{k}_{pq}\right)\tau_{pq}^F \tag{13}$$

where, b considers the virtual mass effect and will be neglected in this study. η_{pq} is the ratio between the Lagrangian integral time scale calculated along particle trajectories, τ^t_{pq} and the characteristic particle relaxation time, τ^F_{pq} and presented as:

$$\eta_{pq} = \tau_{pq}^t \Big/ \tau_{pq}^F \tag{14}$$

Models for b, τ^t_{pq} and τ^F_{pq} are summarized in work of Simonin and Viollet [28].

The transport equation of turbulent kinetic energy dissipation rate $\tilde{\varepsilon}$ should be written in order to achieve full closure. The details of modeling of the $\tilde{\varepsilon}$ with all unknown terms in above equation are available in the work of Cokljat et al. [29].

3. Geometry and Grid Mesh

In this article, a 2D geometry is used in purpose of simulating a bluff body with infinite length. Each grid has three kinds of boundary conditions: velocity inlet, outflow and wall. The wall boundary condition consists of two sides of simulated channel and boundary of bluff body. In order to decrease error and reach the fully developed condition boundary considered far enough from body. The upstream length is 40 times the radius of the cylinder, and the downstream length is 80 times the radius of the cylinder. Also top and bottom walls were considered 30 R away from center of the cylinder. To facilitate meshing, a square with a side length of 20 times the radius of the cylinder is created.around the cylinder and the square is split into four pieces as shown in Fig.1. Figure 1, also shows channel grid and bluff body geometry with applied mesh. Boundary mesh in vicinity of the body is magnified to investigate details of mesh. To make certain grid independency of the results from nodes number, for circular cylinder with D=20 mm, five meshes (40000, 60000, 95000, 115000 and 130000 cells) have been tested. In Fig.2a, b and c drag and lift coefficients and forces have been depicted versus different nodes number for inlet void fraction equal to 0.2. These figures show that the 115000 nodes were least nodes number which the results were totally independent of them. This work was done for other cylinder diameters and geometries, too.

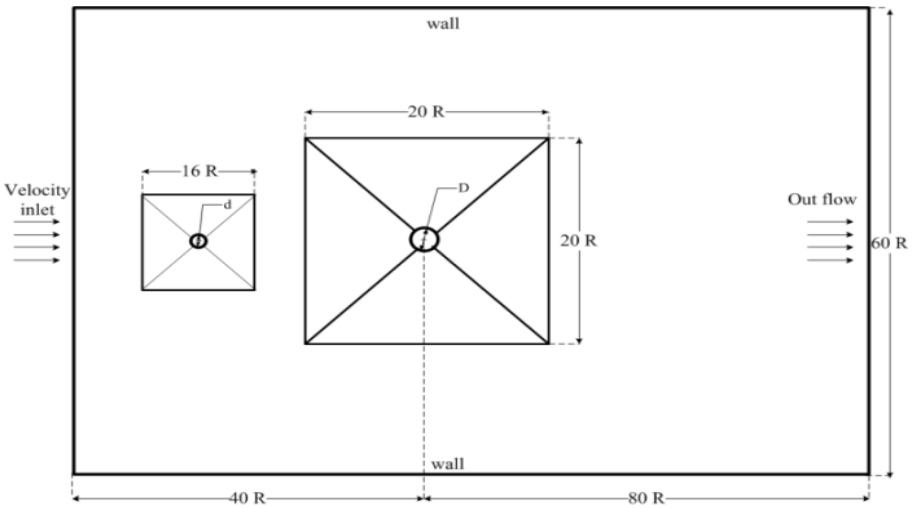

Fig.1a. Schematic of channel and main and auxiliary cylinders with applied boundary conditions.

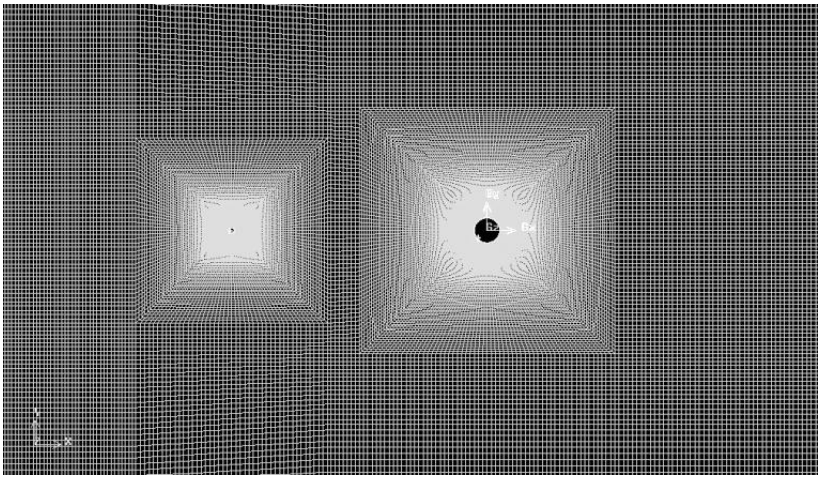

Fig.1b. Applied mesh in the channel and cylinders.

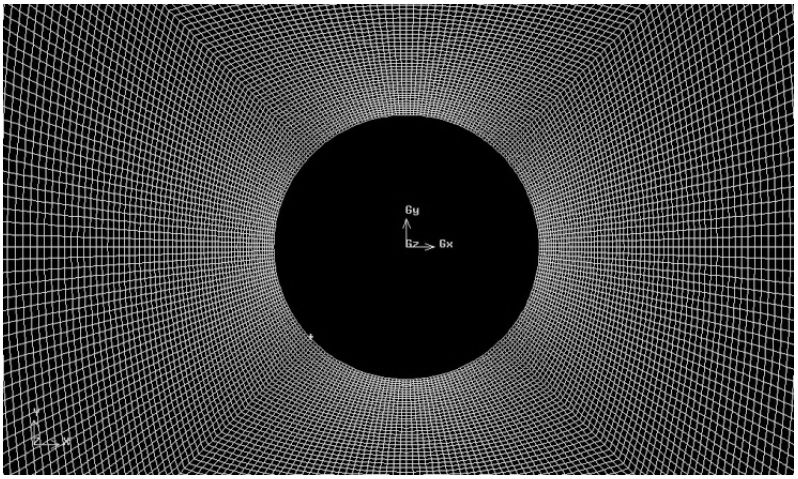

Fig.1c. Magnified mesh around the main cylinder.

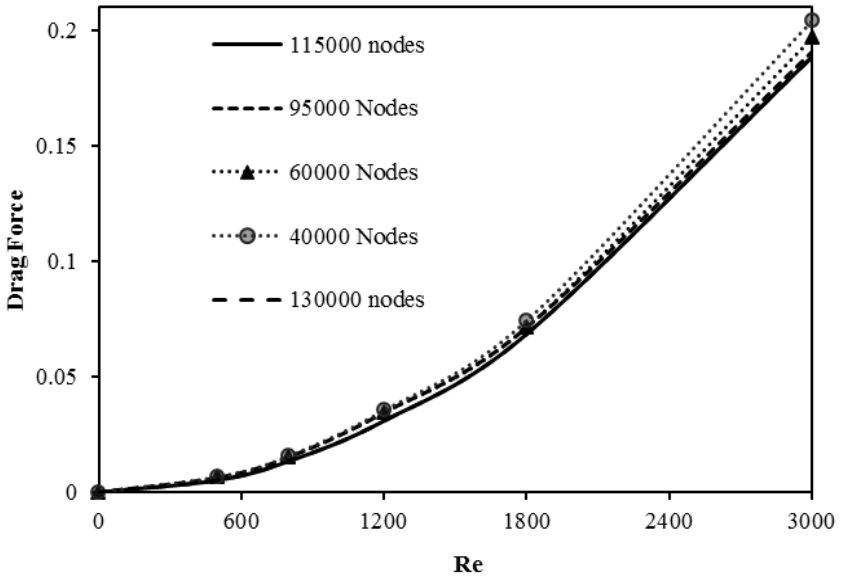

Fig.2a. Validation of mesh independency, drag force vs Reynolds number.

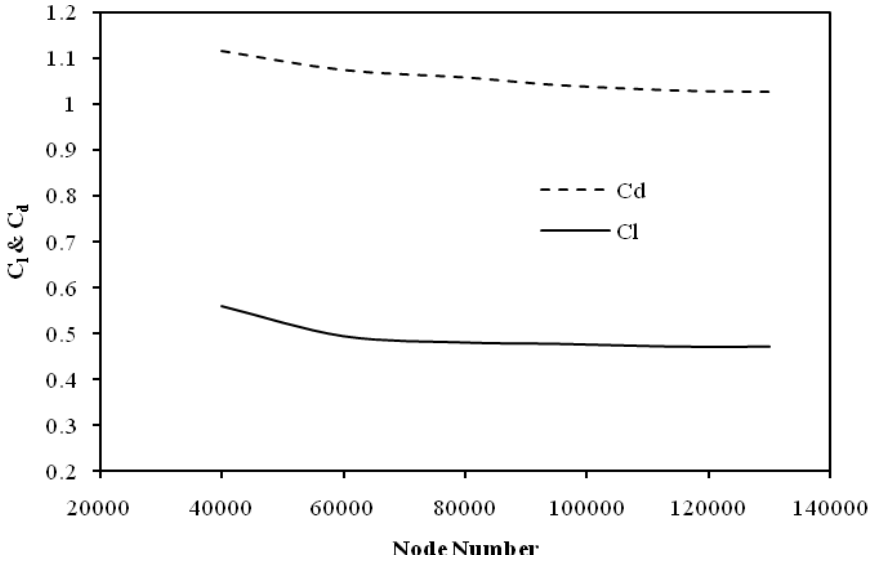

Fig.2b. Validation of mesh independency, drag & lift coefficients vs nodes number.

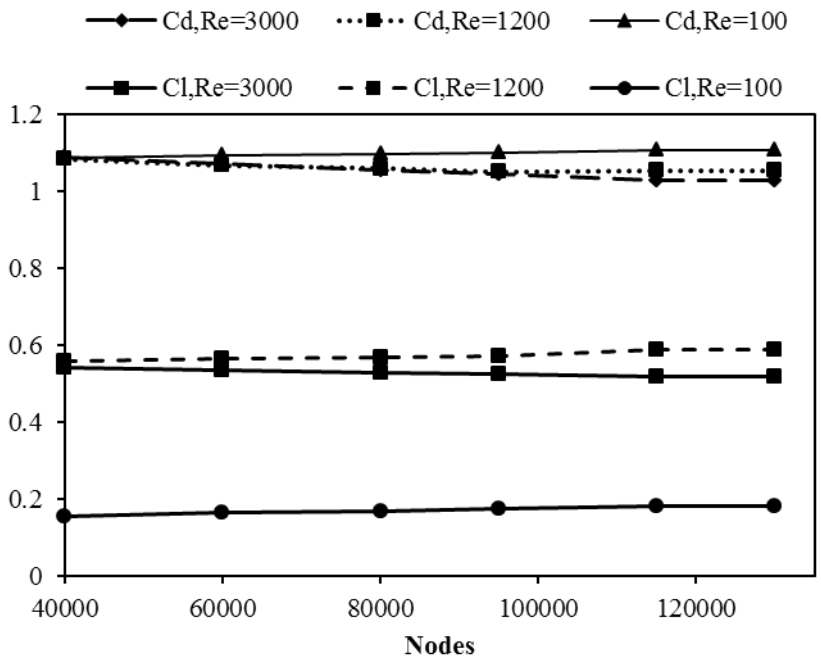

Fig.2c. Validation of mesh independency.

4. Numerical Solution Method

In this study computational method of CFD packag which is used for discretizing the governing equations, is based on the control volume frame work which is proposed by Mathur and Murthy, [30] and Kim et al., [31]. A second order upwind discretization scheme is used to discretize the governing equations. The discretized governing equation is solved using the Phase- Coupled SIMPLE (PC- SIMPLE) algorithm to couple the pressure and velocity fields. A collocated grid is used to all variables stored at the center of control volume. The details of implementation of Reynolds- stress model into single phase were presented in Kim [32]. The details of discretization and multiphase technique are found in Cokljat, [29]. The time dependent equations are solved to increase the stability of the numerical solution. For every iteration the system of two continuity and two momentum equations with the transport equations of turbulent energy and dissipation are solved.

5. Results and Discussion

In this paper the numerical simulation has been carried out for the cylinder with the diameter of 20 mm solely and with sets of revisory cylinders with the diameter ratios of d/D= 0.05, 0.1, 0.15 and 0.20 which are placed with the length to diameter ratios range of L/D= 3- 12 see the Fig.3.

The liquid phase is water and gas phase is considered to be air. The range of void fraction varies between 0.05-0.2, and diameters of bubbles at inlet were considered 1 mm. Moreover Re_{TP} is in range of 100 – 3000, which is defined by

$$Re_{TP} = \left.(\alpha\rho_g + (1-\alpha)\rho_f)vD\right/(\alpha\mu_g + (1-\alpha)\mu_f) \qquad (15)$$

At the first stage, the numerical result of drag coefficient is verified by experimental data [1]. As shown in Fig.4 the predictions are in good agreement with experimental data and the model can predict the overall behavior of it consequently the model has a reasonable accuracy.

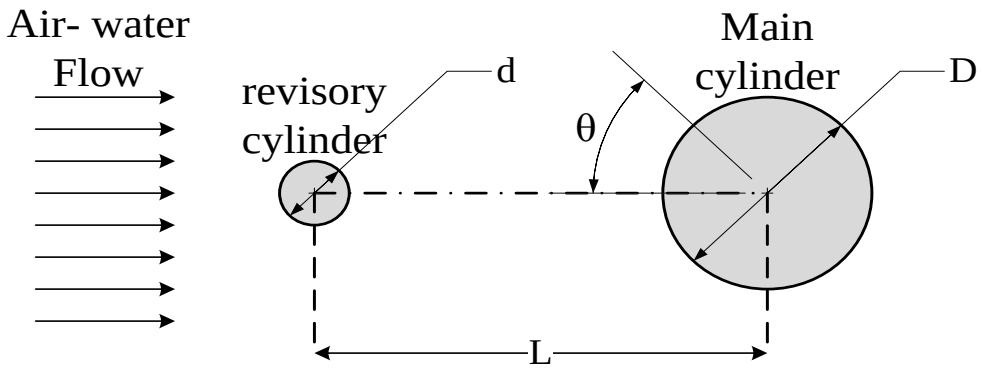

Fig.3. Schematic of flow around main and revisory cylinders.

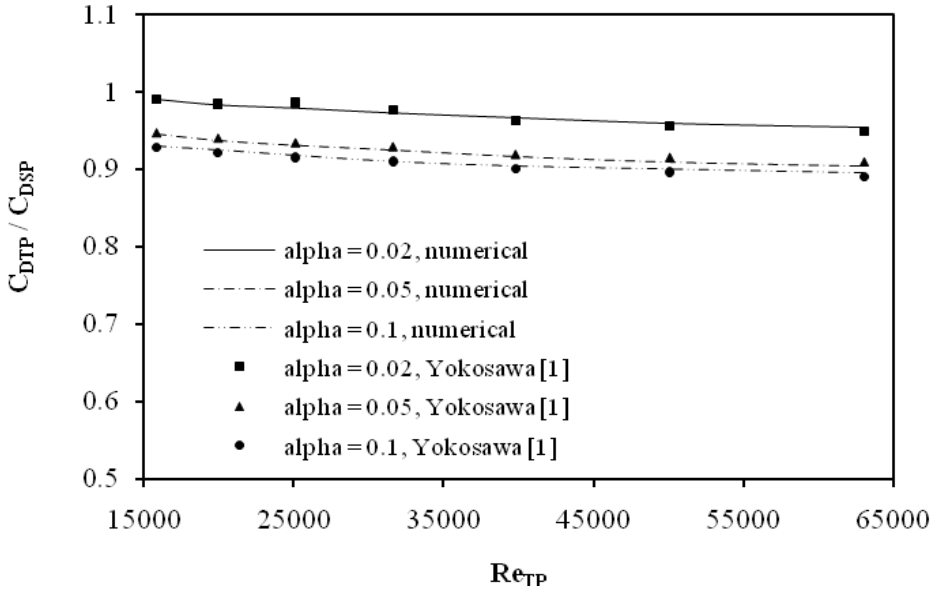

Fig.4. Comparison between experimental results and present work.

Figure 5, shows the variation of lift coefficient versus time for main cylinder without auxiliary rod in inlet air volume fraction of 0.05.

Figure 5, shows that lift coefficient has a fluctuating behavior with time which can lead to resonance phenomenon and tube failure as the result. Therefore in addition to drag and lift coefficient, strouhal number is an important variable to consider as well. Figures 6a and c show the variation of drag coefficient and drag force versus Reynolds number for main cylinder without auxiliary rod at different void fractions. These figures show that increase of void fraction can decrease the total drag force on the cylindrical body at the higher Reynolds number. But it demonstrates in lower Reynolds number. Figure 6b, shows that increase in Reynolds number decreases frictional drag coefficient, therefore in higher Reynolds number pressure drag coefficient becomes more important. This figure also shows that with increase in void fraction, drag coefficient decreases in frictional and pressure drag coefficient. It seems that presence of air bubbles in the vortex of cylinder can lead to reduction in drag coefficient and drag force which is shown in Fig.6c.

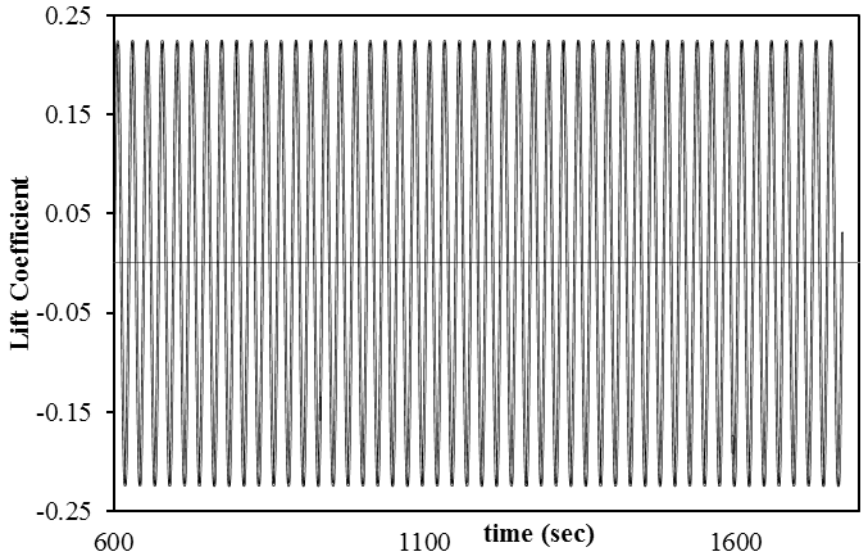

Fig.5. Variation of lift coefficient versus time in Re=100 and void fraction of 0.05.

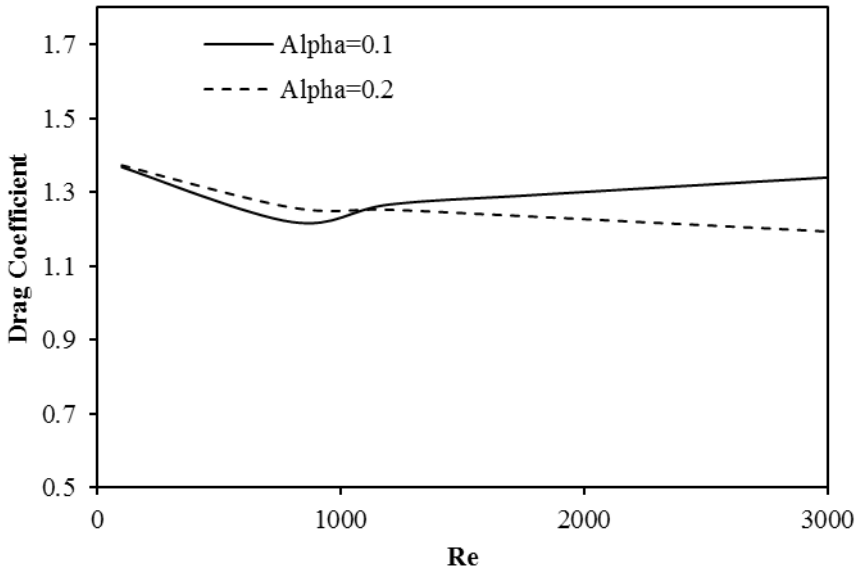

Fig.6a. Variation of drag coefficient versus Reynolds number.

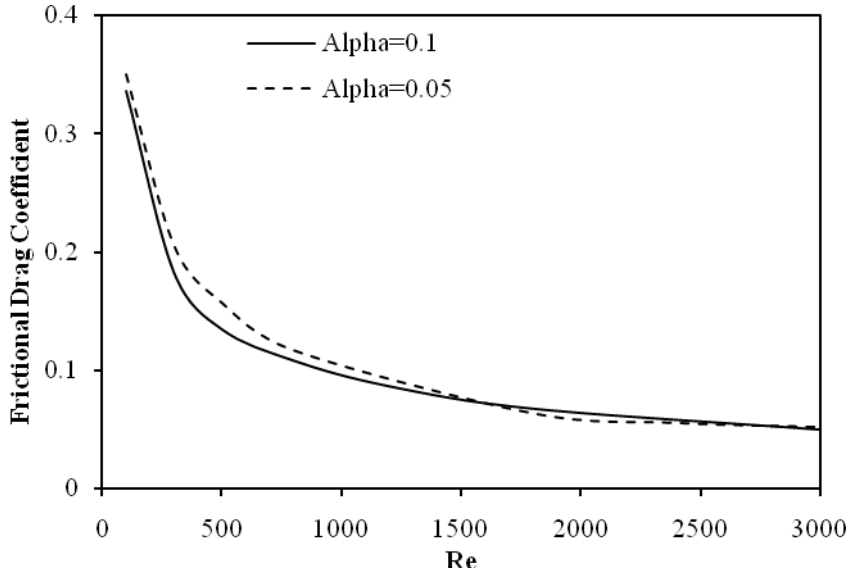

Fig.6b. Variation of drag coefficient versus Reynolds number.

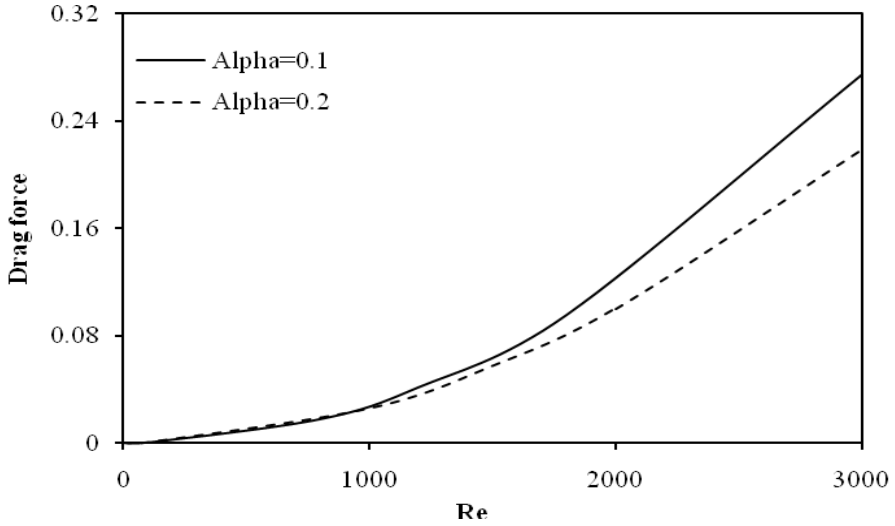

Fig.6c. Variation of drag force versus Reynolds number.

Figure 7, shows the lift coefficient versus Reynolds number for main cylinder without auxiliary rod in air volume fractions of 0.1 and 0.2. It shows that the increase of void fraction decreases the lift coefficient especially in the higher Reynolds numbers. As it is shown in Fig.7 in void fraction equals to 0.2 lift coefficient almost remains unchanged after a specific Reynolds number. It seems that accumulation of air bubbles around the cylinder has the capability to lower the transmitted momentum to cylinder. Variation of lift force versus Reynolds number is illustrated in Fig.8. Figure 8 reveals that lift force decreases with increase of void fraction and it becomes more important in higher Reynolds number as well. Figures 9 and 10 show the distribution of volume fraction of air phase around the cylinder without auxiliary rod for inlet air volume fraction of 0.2 and 0.1, respectively. It is clear that most of the bubbles gathered at the backside of the cylinder. Both figures show that if Reynolds increases the bubbles will move to the forward of the cylinder.

The distribution of volume fraction around the cylinder without auxiliary rod versus Reynolds number is depicted in Fig.11 for three void fractions in Re=3000. Figure 11, shows that in a specific Reynolds number maximum of local volume fraction happens earlier with increase in inlet volume fraction. Figure 12, shows the variation of Strouhal number versus Reynolds number for main cylinder without auxiliary rod in inlet air volume fractions of 0.2 and 0.1. It shows that increase of inlet void fraction decrease the Strouhal number of the cylinder.

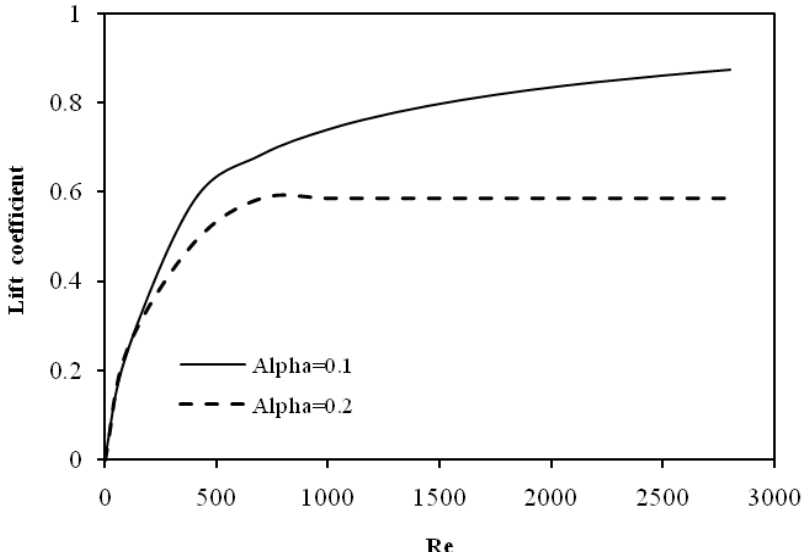

Fig.7. Variation of lift coefficient versus Reynolds number.

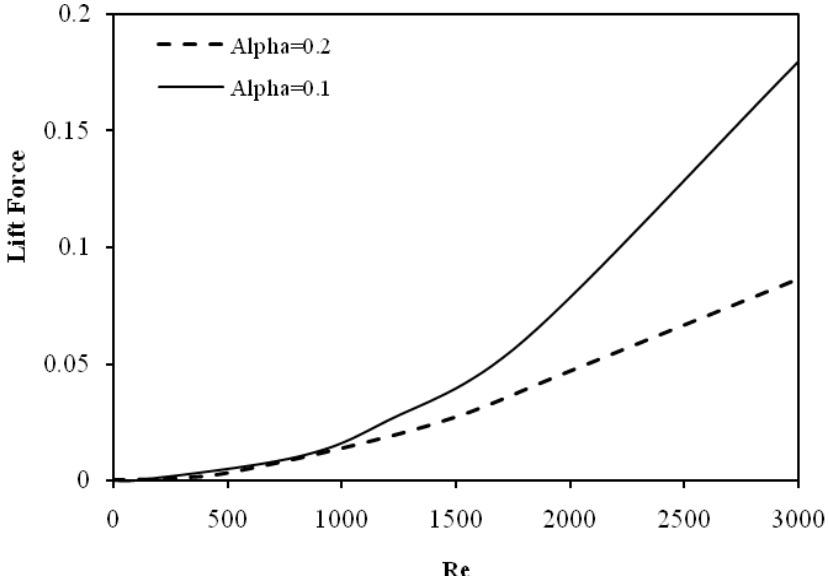

Fig.8. Variation of lift force versus Reynolds number.

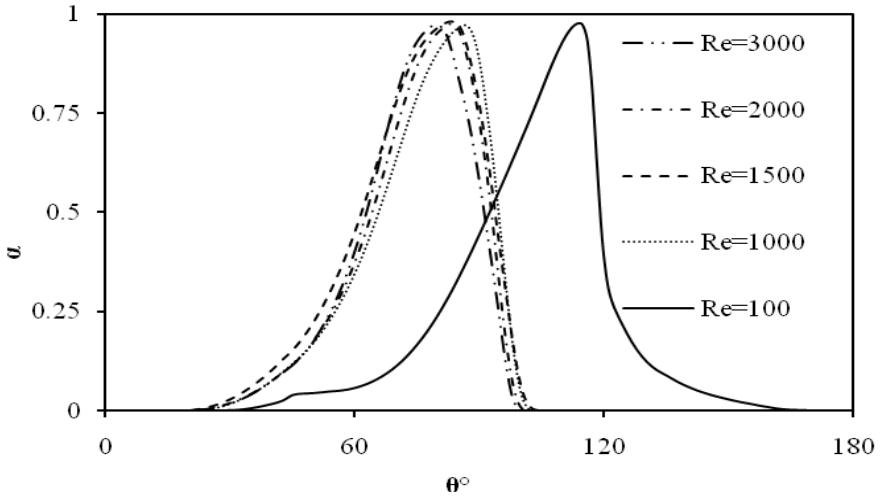

Fig.9. Distribution of volume fraction around main cylinder without auxiliary rod for inlet volume fraction of 0.2.

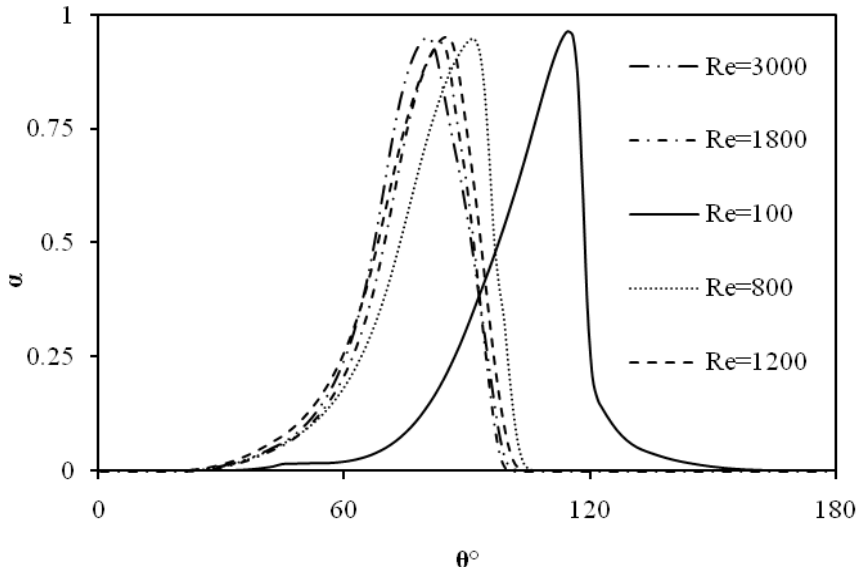

Fig.10. Distribution of volume fraction around main cylinder without auxiliary rod for inlet volume fraction of 0.1.

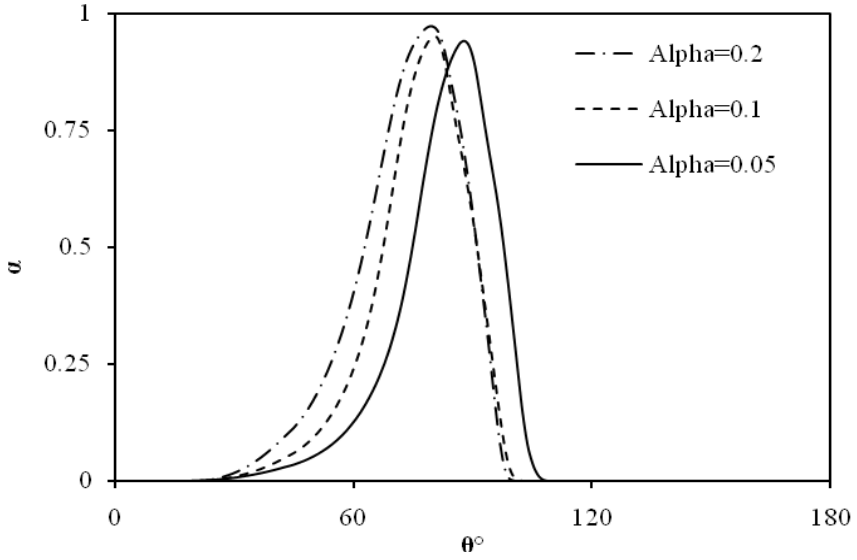

Fig.11. Distribution of volume fraction around main cylinder without auxiliary rod for Re=3000.

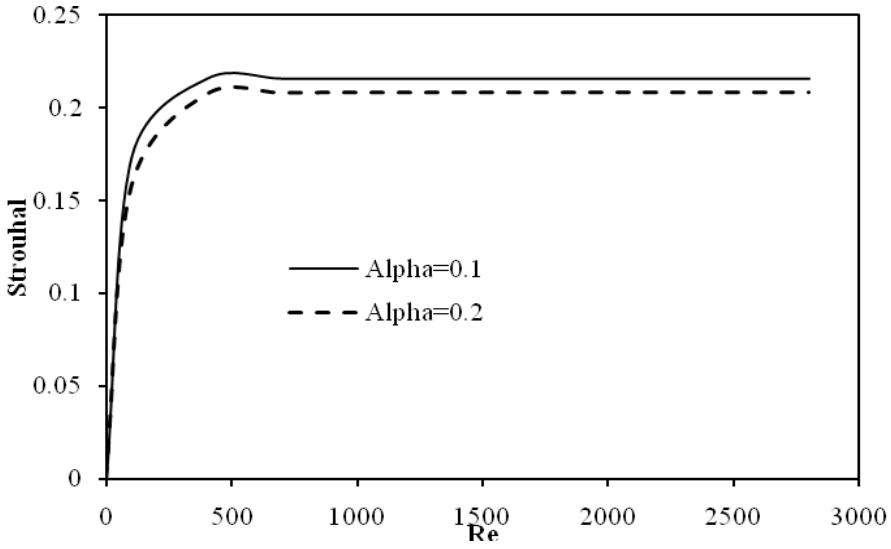

Fig.12. Variation of Strouhal number versus Reynolds number.

For achieving to the optimum geometry, different positions of auxiliary rod with various radiuses were examined and simulated in air- water two phase flows. Figure 13 shows the variation of Strouhal number for different values of d/D and L/D for auxiliary rod. For generalization, the results were depicted in non-dimensional format. The distance of auxiliary rod from the main cylinder, L, and the diameter of the auxiliary rod, d, was none dimensionalized with the diameter of the main rod, D (see Fig.3). It is obvious that increase of the auxiliary rod diameter decreases the Strouhal number and may help main cylinder become more stable but increase of the auxiliary rod diameter will mainly affect the main flow and it is not favorable in the measurement probes but it would be good for the tubes in heat exchangers. The simulated stream lines of the flow around the different auxiliary robs show that the diameter ratio of 0.2 is appropriate for auxiliary rod and its effects on the main flow can be neglected. Figure 13, also reveals that the nearer auxiliary rod to the main cylinder may help it become more stable but as it is clear the auxiliary rod affect the main flow and it is not logical to place it very close to the main cylinder. Figure 14, shows the variation of Strouhal number for different positions of the auxiliary rod for volume fraction of 0.05. This figure indicates that the best position for placing the auxiliary rod is in the L/D= 10 which has the lowest Strouhal number. This shows that in this position the main cylinder would have the lowest vortex shedding and become more stable. In this study the stream lines of the different positions of the auxiliary rod show that the best place for auxiliary rod is in the L/D= 10.

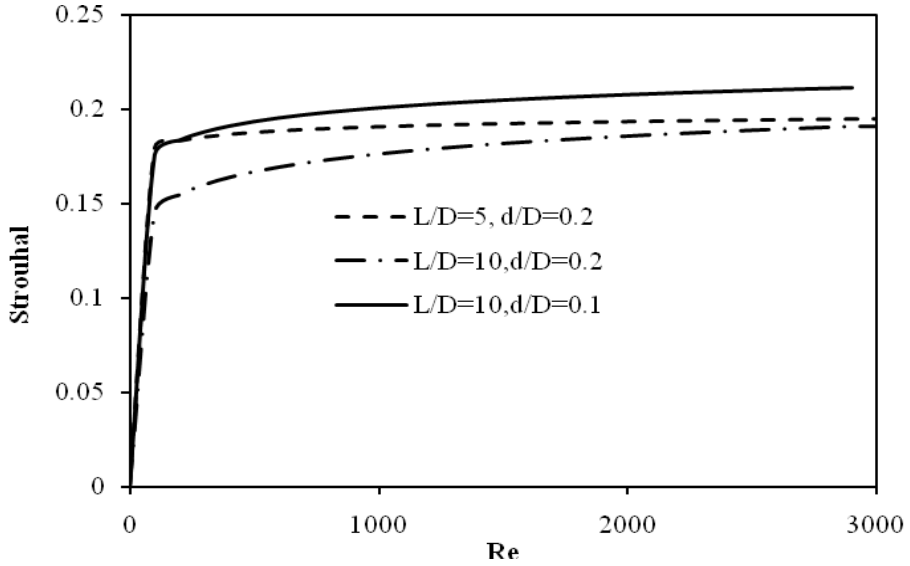

Fig.13. Variation of Strouhal number versus Reynolds number in presence of revisory rod in inlet void fraction of 0.2.

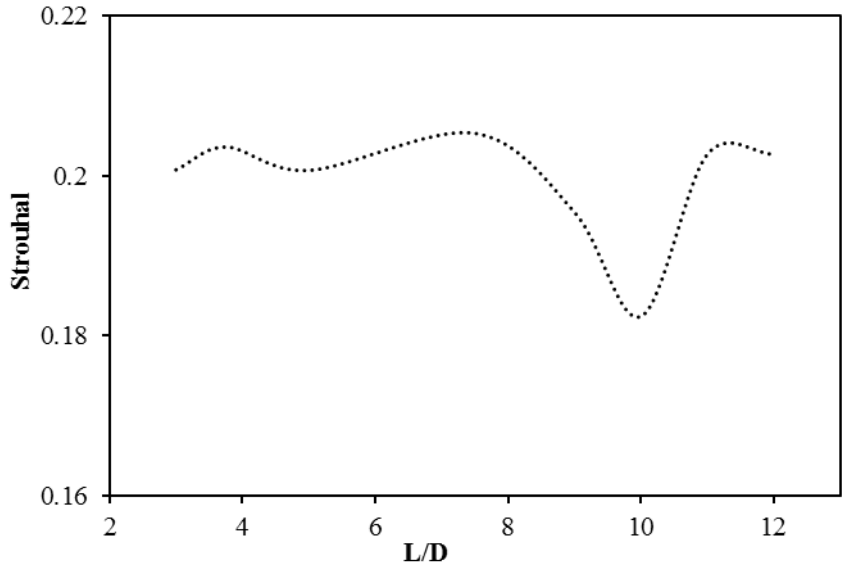

Fig.14. Variation of Strouhal number for different position of auxiliary rod from the main cylinder in volume fraction of 0.05 at Re=800.

Figure 15, shows the variation of Strouhal number versus Reynolds number for cylinder with auxiliary rod placed in the L/D= 10 with diameter ratio of d/D= 0.2 for three void fractions; 0.05, 0.1 and 0.2. Similar to the results for the cylinder without auxiliary rod, increase in inlet air void fraction decreases the Strouhal number and it shows that the higher void fraction can help the cylinder become more stable. It seems that air bubbles accumulate at the back of the cylinder and decrease the vortex shedding frequency around it.

Figure 16, shows the comparison of Strouhal number for main cylinder with and without rod versus Reynolds number. This figure reveals that the auxiliary rod placed in the position of L/D= 10 can decrease the Strouhal number of the main cylinder. It means that in this case the vortex shedding occurs less than the cylinder without auxiliary rod. The difference between the values of Strouhal number for cylinder with and without auxiliary rod increases with increase of the Reynolds number.

Therefore, the auxiliary rod can help the cylinder become more stable especially in the high Reynolds flows.

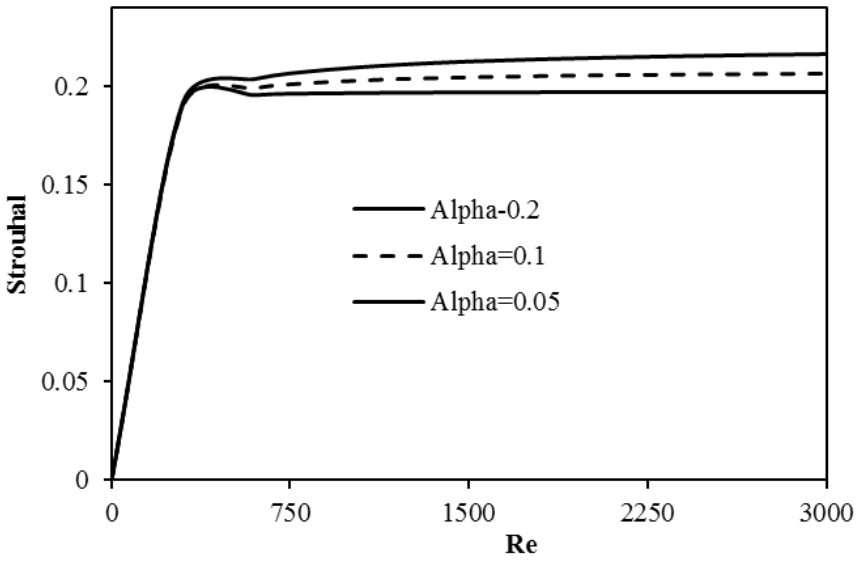

Fig.15. Variation of Strouhal number for cylinder with auxiliary rod.

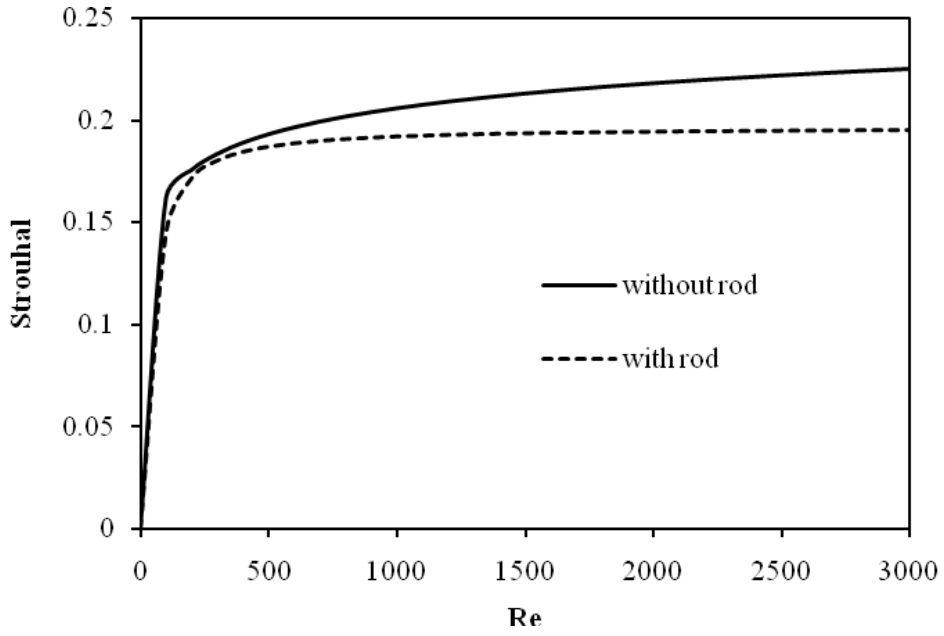

Fig.16. Comparison of strouhal number with and without revisory rod.

Figure 17, shows the variation of lift coefficient versus Reynolds number for main cylinder with auxiliary rod placed at the position of L/D=10 with diameter ratio of d/D= 0.2. Like the behavior of the lift coefficient for cylinder without auxiliary rod, increase of inlet air volume fraction decreases the lift coefficient due to the accumulation of the bubbles behind the cylinder. Figures 19-20 show the variation of pressure coefficient around main cylinder with auxiliary rod placed at the optimum distance for inlet air volume fractions of 0.2 and 0.1, respectively.

Increase of Reynolds number from 100 to 3000 decreases the value of the pressure coefficient. This behavior was seen in the air- water two phase flows around the cylinder without auxiliary rod.

The concentration of bubbles in the low pressure region (backside) of the cylinder increases the local pressure in that region and causes the lower pressure coefficient and pressure drag for cylinder. The behavior of the pressure coefficient variation with Reynolds number is not a unique trend and varies with inlet void fraction.

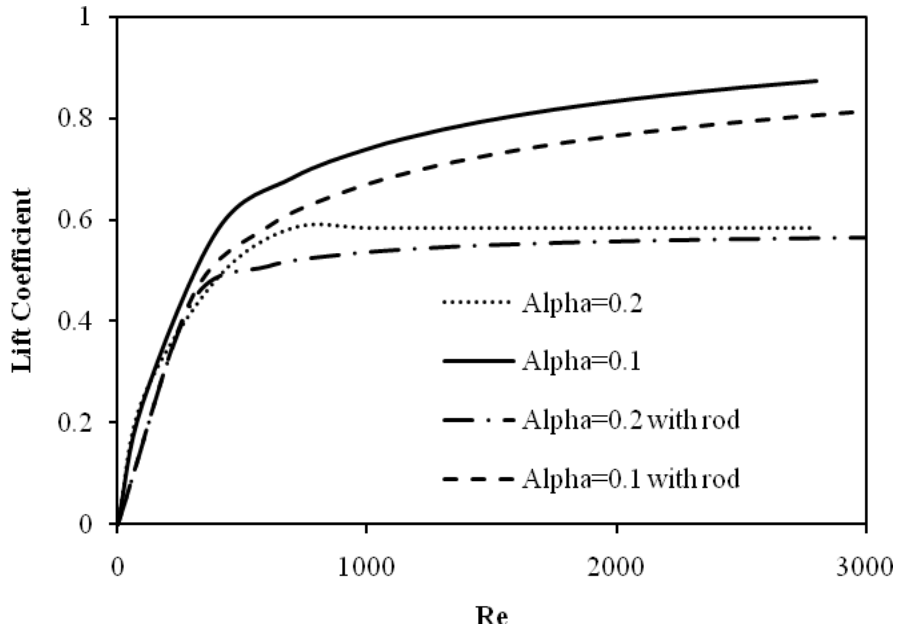

Fig.17. Comparison of lift force with and without revisory rod.

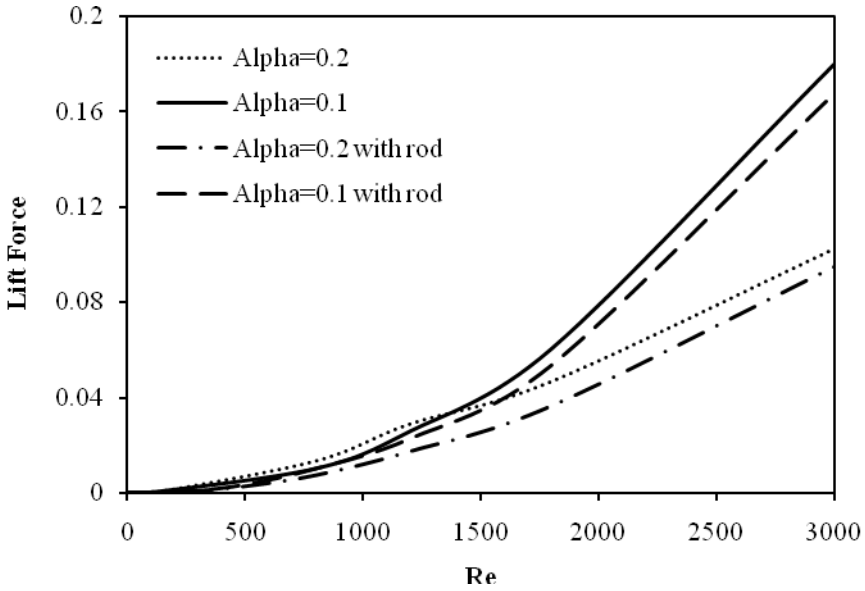

Fig.18. Comparison of lift coefficient with and without revisory rod.

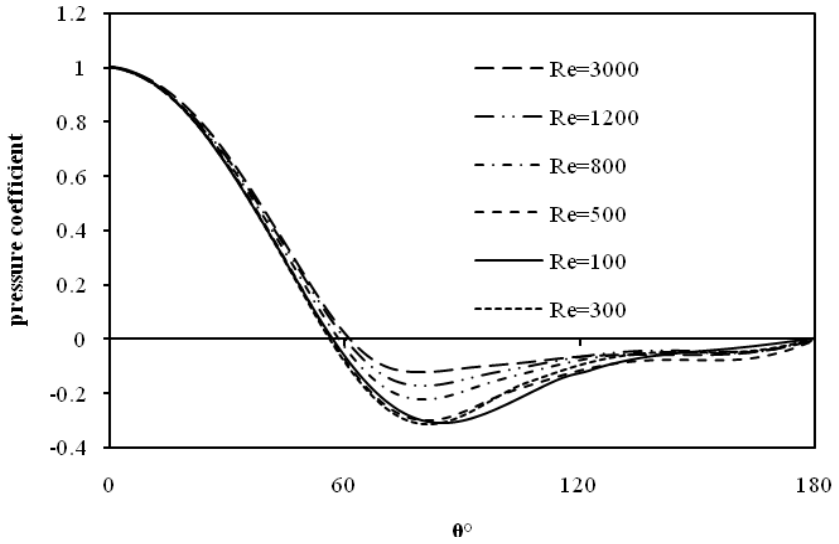

Fig.19. Variation of pressure coefficient around main cylinder with auxiliary rod in volume fraction of 0.2.

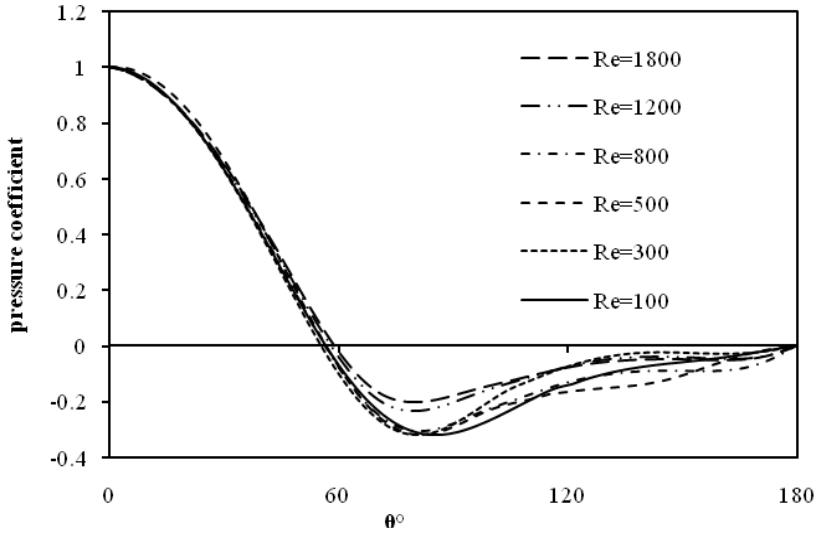

Fig.20. Variation of pressure coefficient around main cylinder with auxiliary rod in volume fraction of 0.1.

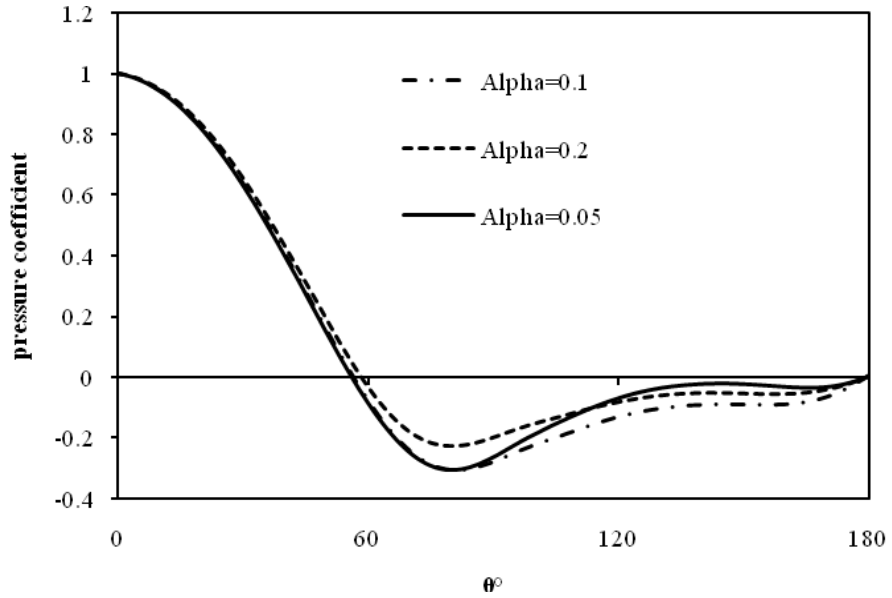

Fig.21. Variation of pressure coefficient around cylinder with auxiliary rod at Re=800.

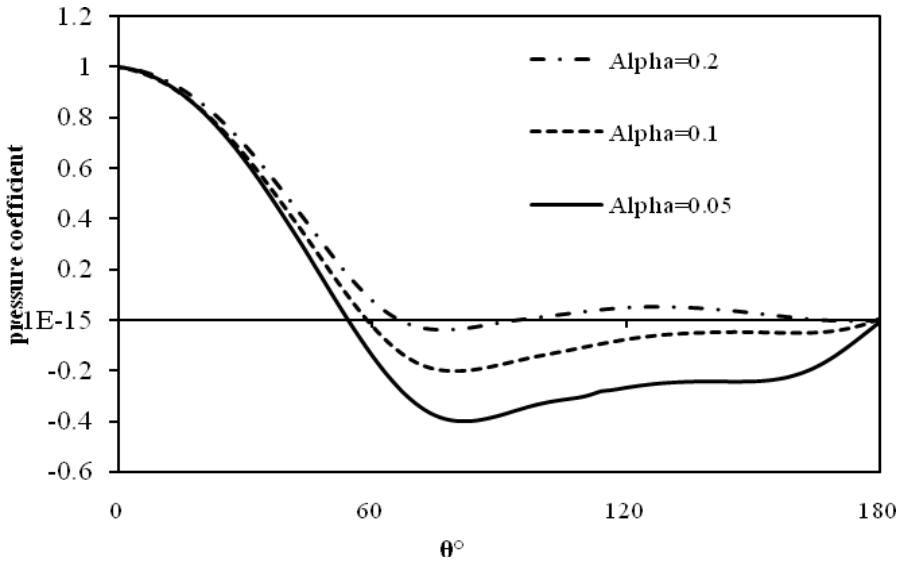

Fig.22. Variation of pressure coefficient around cylinder with auxiliary rod at Re=1800.

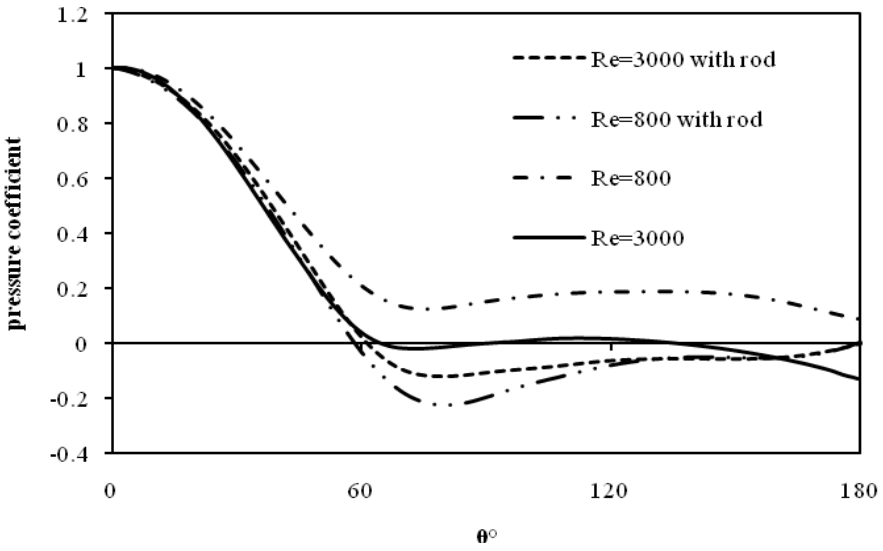

Fig.23. Comparison of pressure coefficient after and before placing revisory rod in inlet volume fraction of 0.2.

Figures 24-26 show the variation of volume fraction around the cylinder with auxiliary rod for different Reynolds numbers in inlet air volume fractions of 0.05, 0.1 and 0.2 respectively.

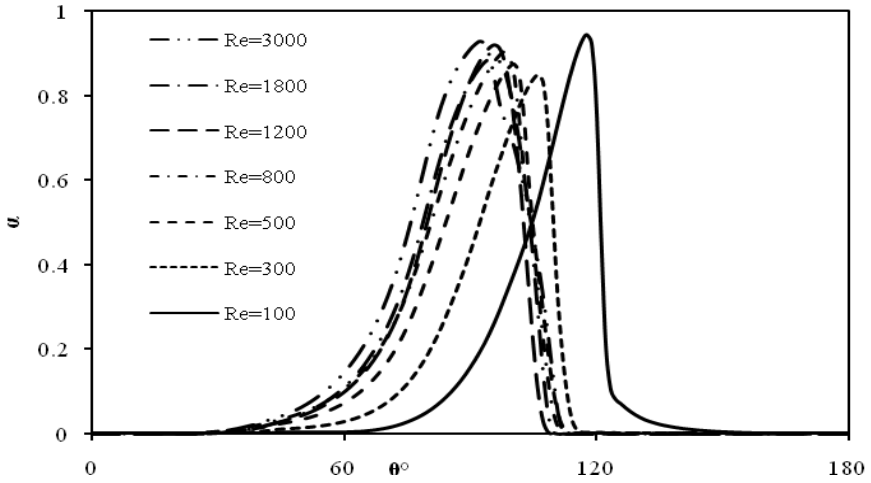

Fig.24. Variation of volume fraction around cylinder with auxiliary rod in inlet air volume fraction of 0.05.

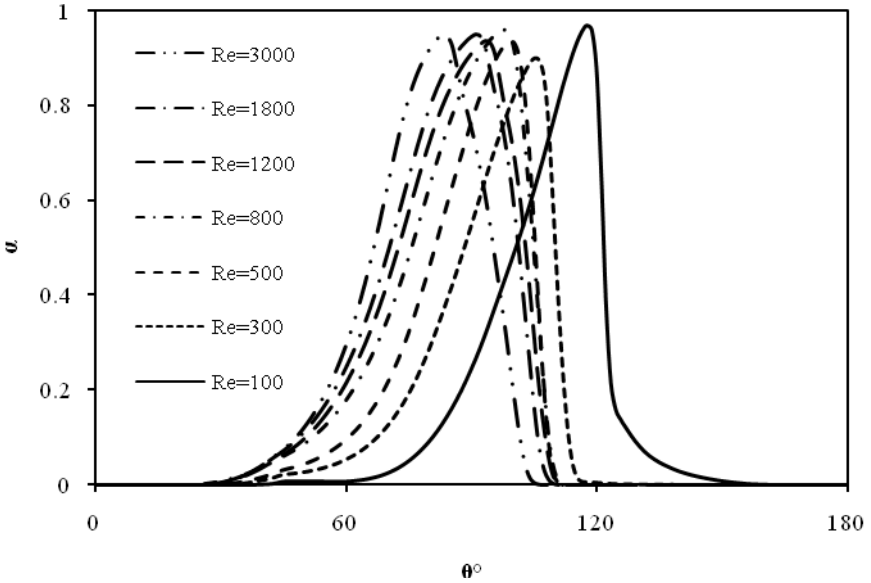

Fig.25 .Variation of volume fraction around cylinder with auxiliary rod in inlet air volume fraction of 0.1.

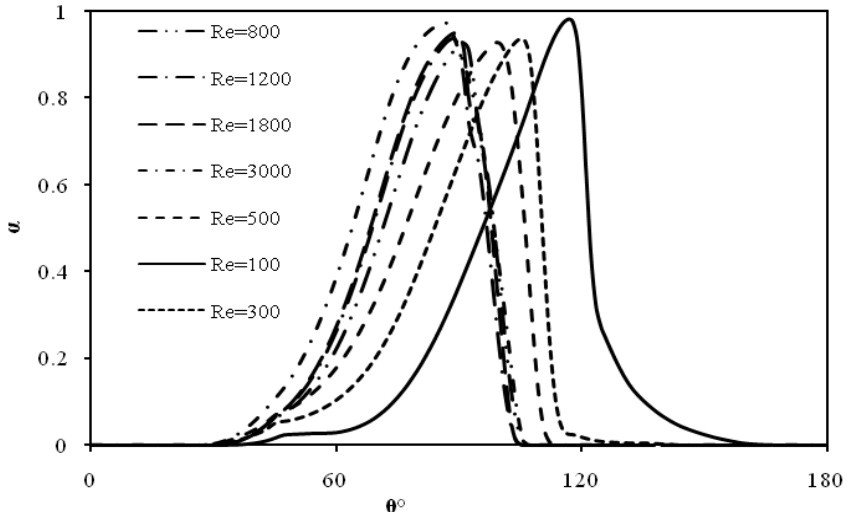

Fig.26. Variation of volume fraction around cylinder with auxiliary rod in inlet air volume fraction of 0.2.

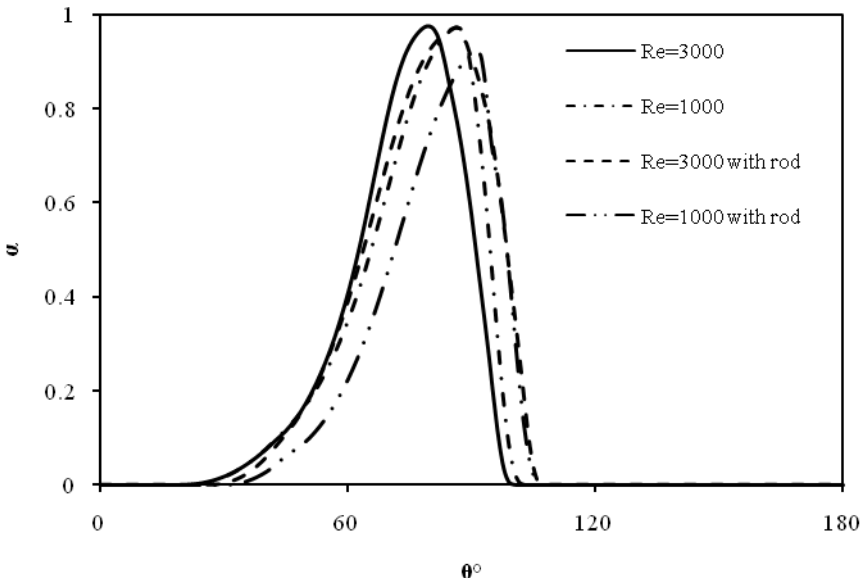

Fig.27. Variation of volume fraction around cylinder with and without auxiliary rod in inlet air volume fraction of 0.1.

Figures 28 and 29 illustrate variation of volume fraction around cylinder with auxiliary rod for three different inlet void fractions at Re=1800 and Re=100, respectively. These figures confirm that the overall behavior of the flow before and after of placing rod is still alike.

Figure 30, shows the distribution of air volume fraction around cylinder with and without auxiliary rod for two inlet void fractions of 0.1 and 0.2 at Re=3000. It can be deduced from Fig.30 that in presence of auxiliary rod maximum value of volume fraction around the cylinder happens later.

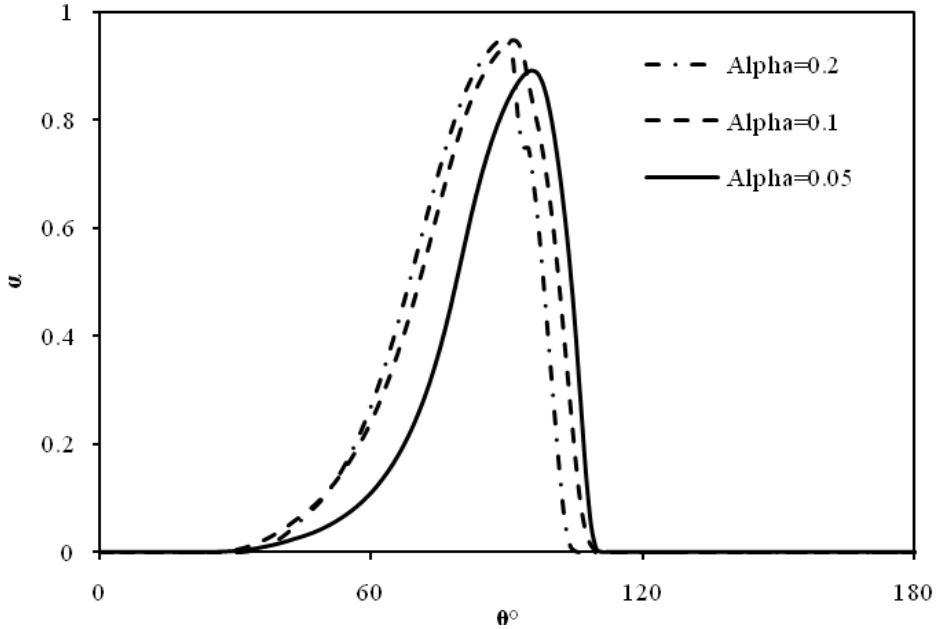

Fig.28. Variation of volume fraction around cylinder with auxiliary rod at Re=1800.

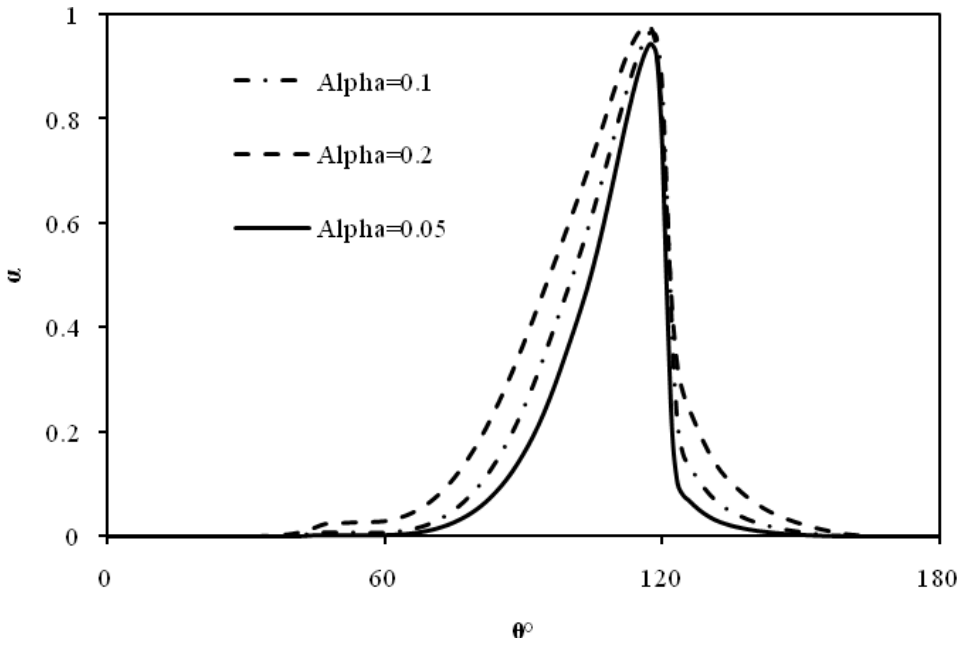

Fig.29. Variation of volume fraction around cylinder with auxiliary rod at Re=100.

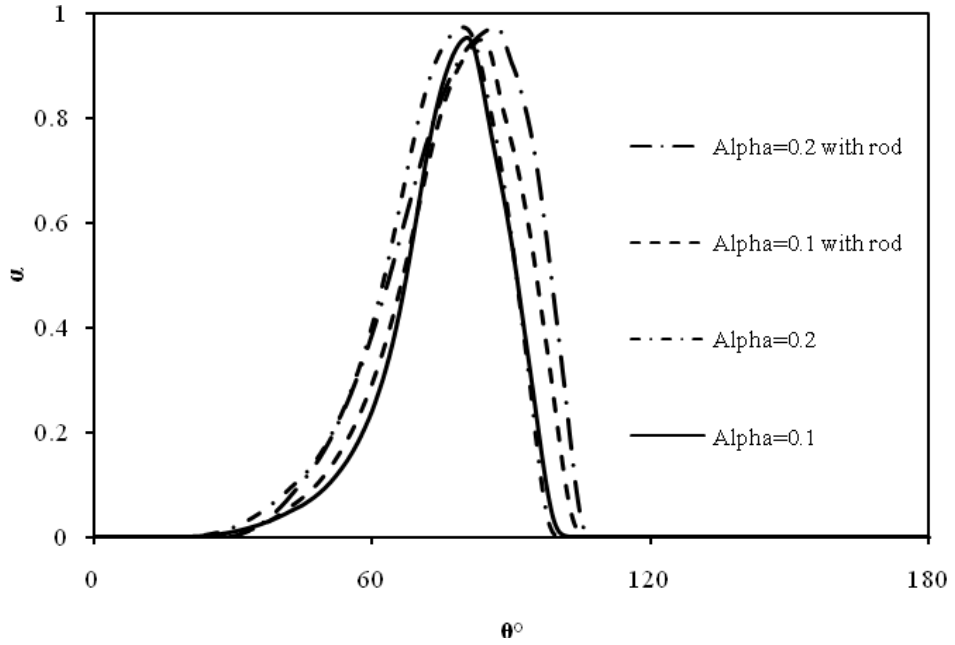

Fig.30. Variation of volume fraction around cylinder with and without auxiliary rod at Re=3000.

Figure 31, shows the drag coefficient versus Reynolds number with revisory rod for three different inlet void fractions of 0.05, 0.1 and 0.2. It reveals that increase of void fraction decreases the drag coefficient. Figure 32, also illustrates the frictional drag coefficient versus Reynolds number with revisory rod for three different inlet void fractions of 0.05, 0.1 and 0.2. It is obvious that increase of void fraction decreases the overall two phase flow density which leads to decrease frictional drag force.

Figures 33 and 34 show the comparison of drag coefficient and drag force for a cylindrical tube with and without auxiliary rod. The comparisons show that placing an auxiliary rod can help in decreasing the drag force on the main cylindrical tube. The void fraction contour around the cylinder is depicted in Fig 34, for various Reynolds numbers. It is noticed that increase of velocity spread the bubbles at the backside wake. In high Reynolds flow bubbles concentration is distinguished at the wake.

Figures 35a-d show the void fraction contours for cylinder without auxiliary rod while Figures 35e-h illustrate it for cylinder with auxiliary rod.

Figures 36a-c represent the stream lines, velocity contour and an experimental real photo for air- water two phase flows around the main cylinder.

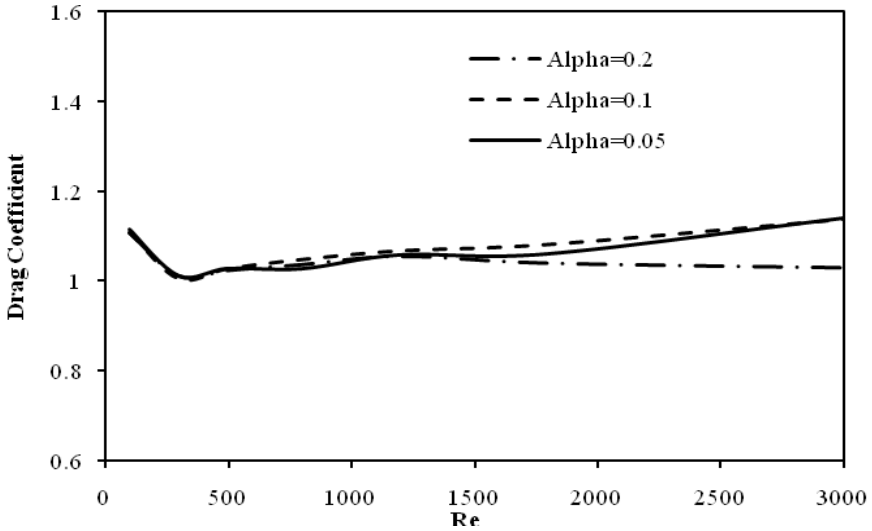

Fig.31. Drag coefficient versus Reynolds number with revisory rod.

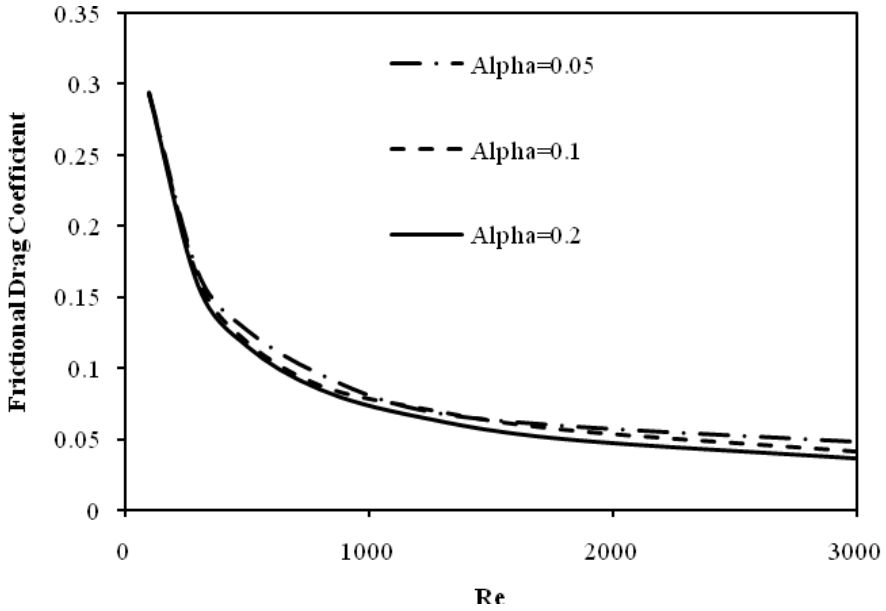

Fig.32. Frictional drag coefficient with revisory rod.

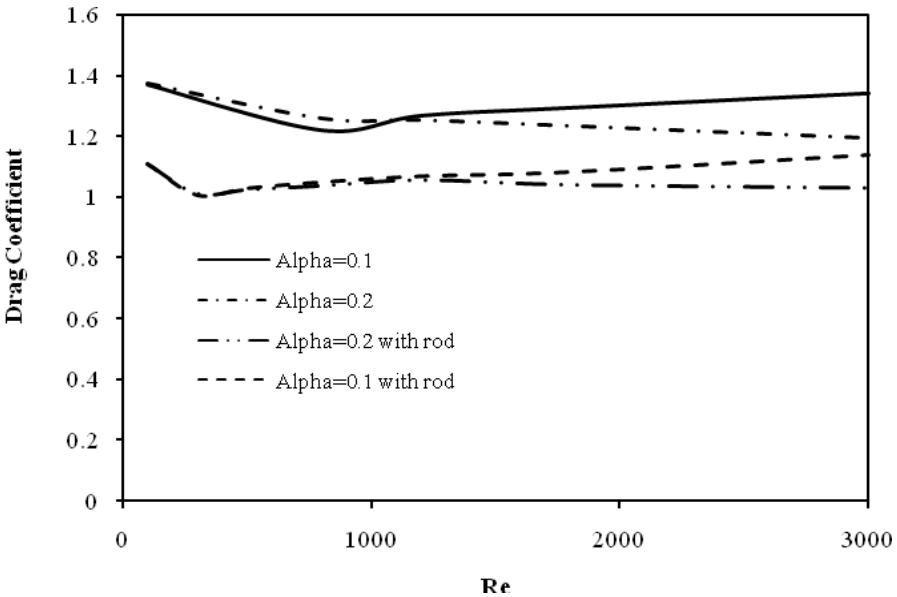

Fig.33. Comparison of drag coefficient with and without revisory rod

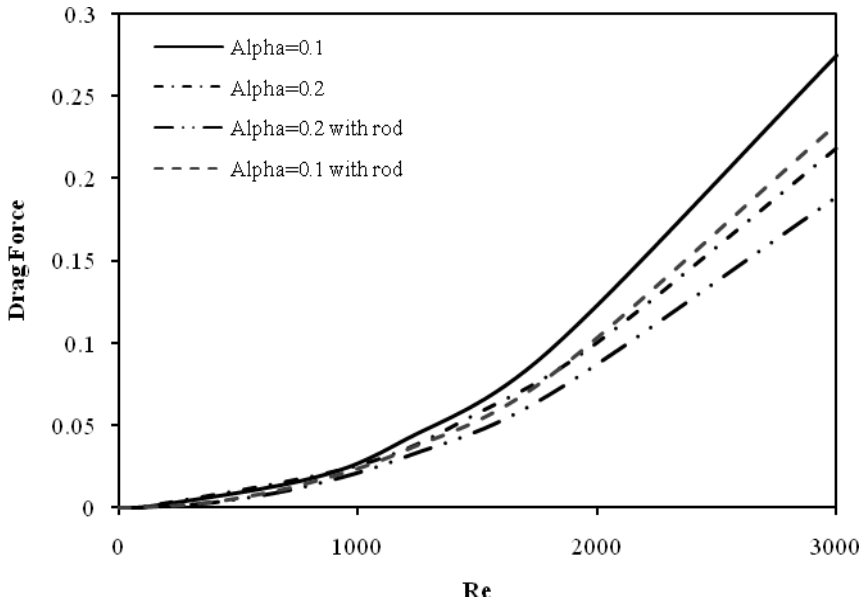

Fig.34. Comparison of drag coefficient with and without revisory rod.

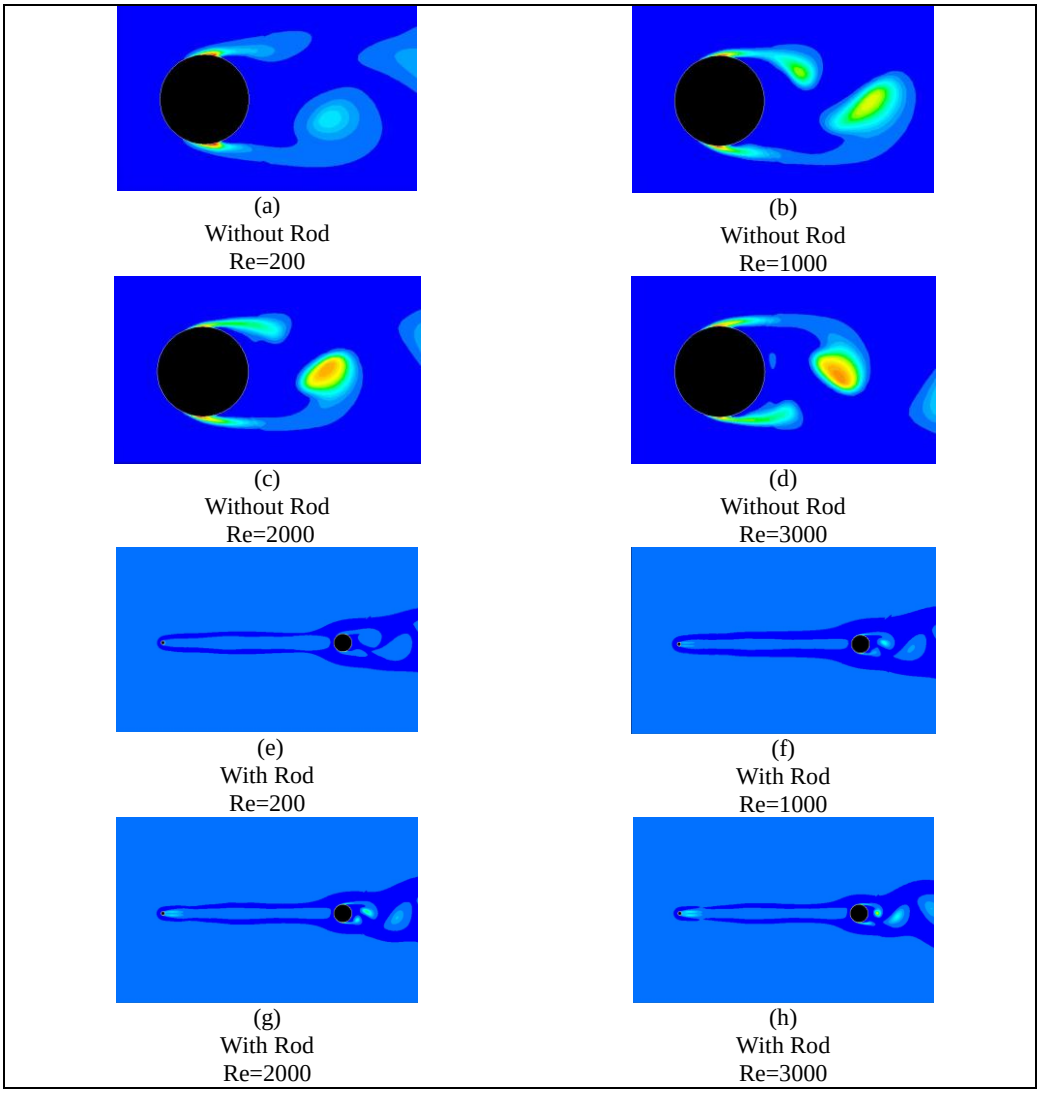

Fig.35. Air- water two phase flow void fraction contour around cylinder

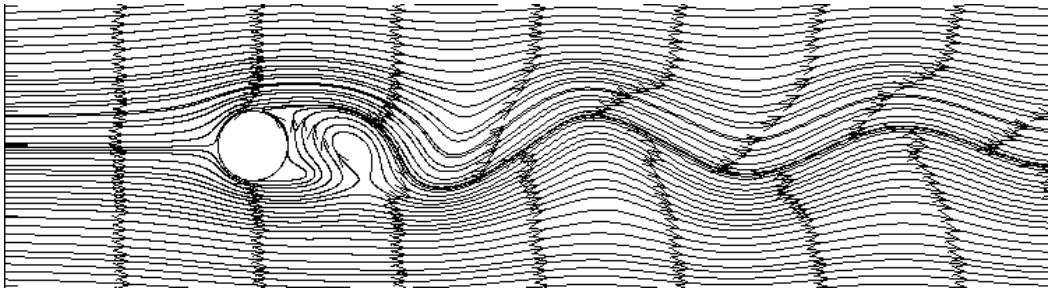

a) Air- water two phase flow stream lines.

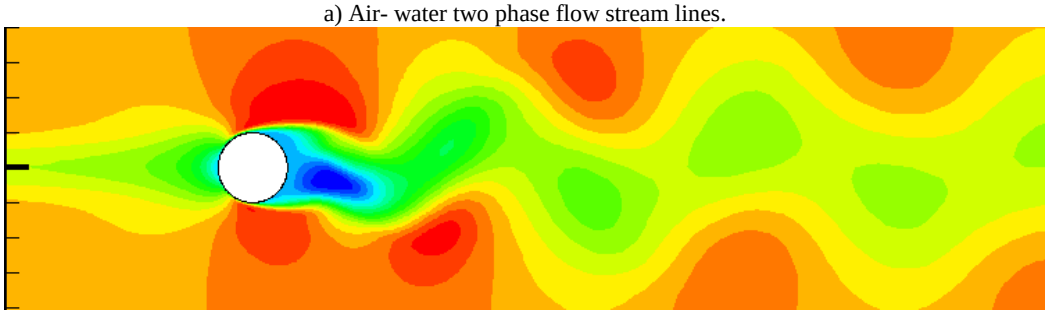

b) Air-water two phase flow velocity contour.

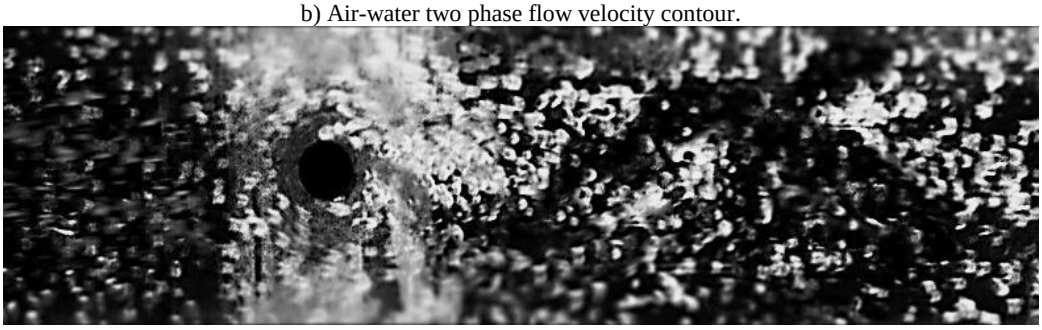

c) Photo of air- water flow around a cylindrical tube.

Fig.36. The stream lines and velocity contour around cylinder.

6. Conclusions

In this paper, a numerical approach is used to predict drag and pressure coefficient in air- water two- phase flow around the cylindrical tube. The current data compared with experimental data to validate the numerical simulation. It is shown that pressure coefficient decreases with increase in void fraction especially at the separation point. The results show that the overall behavior of pressure coefficient variation is same as single phase flow. The result also illustrated that the lift coefficient decreases with increase in void fraction. Increase in velocity causes the bubbles accumulate into the wake at the backside of the body. The result indicated that the auxiliary rod placed in front of the main cylinder can help the main cylindrical tube be more stable and decreases the Strouhal number. The results indicated that the best position for the auxiliary rod is in the L/D= 10 and the optimum diameter ratio for rod is d/D= 0.2. Simulation of air- water two phase flow shows that the concentration of the bubbles around the cylinder with auxiliary rod happens later in the backside of the cylinder. It follows the lower lift coefficient and Strouhal number for the main cylinder tube.

Nomenclature

C	constant
D	diameter
F	force
G	Gravity
H	width of channel
K	interphase momentum exchange coefficient
k	turbulent kinetic energy
L	up riser tube length
m	mass flow rate
p	pressure
R	inter-phase force
S	source term
t	time
v	velocity
V	volume of phase

Greek symbols

α	void fraction
λ	bulk viscosit
μ	shea viscosity
ρ	density

τ	stress-strain tensor
ε	turbulent dissipation

Subscribe

i	initial
p	primary phase
q	secondary phase

References

[1] Yokosawa, M., Kozawa, Y., Inoue, A. and Aoki, S., 1986, "Studies on Two-Phase Cross Flow, Part II: Transition Reynolds Number and Drag Coefficient," Int. J. of Multiphase Flow, 12, 2, 169-184.

[2] Inoue, A., Kozawa, Y., Yokosawa, M. and Aoki, S., 1986, "Studies on Two-Phase Cross Flow, Part I: Flow Characteristics around a Cylinder," Int. J. of Multiphase Flow, 12, 2, pp. 149-167.

[3] Pettigrew, I. J., Tromp, J. H., Taylor, C. E. and Kim, B. S., 1988, "Vibration of Tube bundles in two-phase cross-flow, Part 2: fluid-elastic instability," ASME Int. Syrup. On Flow-Induced Vibrations and Noise, Winter Annual Meeting, Chicago, 3, 159-179.

[4] Joo, Y. and Dhir, V. K., 1994, "An Experimental Study of Drag on a Single Tube and on a Tube in an Array under Two-Phase Cross Flow," Int. J. of Multiphase Flow, Vol. 20, No. 6, pp. 1009-1019.

[5] Hara, F. and Ohtani, I., 1982, "Vibration of Circular Cylinder in Cross Two-Phase Flow (1st report; Karmann Vortex Shedding and Pressure Fluctuations)," Tran. JSME, Vol. 48, pp. 962-971.

[6] Hara, F., 1982, "Two-Phase Cross Flow Induced Vibration in a Cylindrical System (2nd report, Characteristics of Unsteady Lift and Drag Force)," Tran. JSME, Vol. 48, pp. 1371-1379.

[7] Hulin, J. P., Fierfort, C. and Coudol, R., 1982, "Experimental Study of Vortex Emission Behind bluff Obstacles in Gas Liquid Vertical Two-Phase Flow," Int. J. of Multiphase Flow, 8, 475-490.

[8] Artemiev, V. K. and Kornienko, Yu. N., 2002, "Numerical modeling of influence non-monotonic profile of gas (vapor) content on a distribution of velocity and temperature in a two-phase bubbly flow," Proceedings, 3rd Russian National Conference on Heat Transfer, Moscow, Russia, Vol. 5, pp. 41–44.

[9] Zaichik, L. I., Skibin, A. P., Soloviev, S. L., 2004, "Simulation of the distribution of bubbles in a turbulent liquid using a diffusion-inertia model," Int. J. of High Temp., Vol. 42, pp. 111–118.

[10] Kamp, A., Colin, C., Fabre, J., 1995, "The local structure of a turbulent bubble pipe flow under different gravity conditions," Proceedings, 2nd International Conference on Multiphase Flow, Kyoto, Japan, Vol. 3, Paper No. P6.

[11] Antal, S. P., Lahey Jr., R. T., Flaherty, J. F., 1991, "Analysis of phase distribution in fully developed laminar bubbly of two-phase flow," Int. J. of Multiphase Flow, Vol. 17, pp. 363–652.

[12] Lopez, M. A., Lahey Jr., R. T., Jones, O. C., 1994, "Phase distribution in bubbly two-phase flow in vertical ducts," Int. J. of Multiphase Flow, Vol. 20, pp. 805–818.

[13] Carrica, P. M., Drew, D. A., Bonetto, F., Lahey Jr., R. T., 1999, "A polydisperse model for bubbly two-phase flow around surface ship," Int. J. of Multiphase Flow, Vol. 25, pp. 257–305.

[14] Politano, M. S., Carrica, P. M., Converti, J., 2003, "A model for turbulent polydisperse two-phase flow in vertical channel," Int. J. of Multiphase Flow, Vol. 29, pp.1153–1182.

[15] Troshko, A. A. and Hassan, Y. A., 2001, "A two-equation turbulence model of turbulent bubbly flow," Int. J. of Multiphase Flow, Vol. 27, pp. 1965–2000.

[16] Lee, S. L., Lahey Jr., R. T., Jones, O. C., 1989, "The prediction of two-phase turbulence and phase distribution phenomena using a $k-\epsilon$ model," Japan J. of Multiphase Flow, Vol. 3, pp. 335–368.

[17] Ghanbarzadeh, S., Hanafizadeh, P., Saidi, M. H., "Time-Average Drag Coefficient and Void Fraction in Gas-Liquid Two Phase Cross Flow,"Proceedings of FEDSM2009ASME 2009 Fluids Engineering Division Summer MeetingAugust 2-5, 2009, Vail, Colorado USA.

[18] Dhotre, T. and Joshi, J., B., 2007, "Design of a gas distributor: three-dimensional CFD simulation of a coupled system consisting of a gas chamber and a bubble column," Chem. Eng. Journal, Vol. 125, pp. 149–163.

[19] Dhotre, M., T., Niceno, B., N., Smith, B., L., 2007, "Large eddy simulation of a bubble column using dynamic sub-grid scale model," Chem. Eng. Journal.

[20] Lehr, F., Millies, M., and Mewes, D., 2002, "Bubble-Size Distributions and Flow Fields in Bubble Columns," A.I.Ch.E. Journal, Vol. 48, pp. 2426-2443.

[21] Mudde, R. F., Lee, D. J., Reese, J., and Fan, L. S., 1997, "Role of Coherent Structures on Reynolds Stresses in a 2-D Bubble Column," A.I.Ch.E. Journal, Vol. 43, pp. 913–926.

[22] Simonin, O., 1990, "Eulerian Formulation for Particle Dispersion in Turbulent Two-Phase Flows," Proceedings, Fifth Workshop on Two-Phase Flow Predictions, Erlangen, Germany.

[23] Anderson, T. B. and Jackson, R., 1967, "A Fluid Mechanical Description of Fluidized Beds." I & EC Fundamental, 6, 527-534.

[24] Bowen, R. M., 1976, "Theory of Mixtures," Continuum Physics, Academic Press, pp. 1-127, New York.

[25] Schiller, L. and Naumann, Z. 1935, "A drag coefficient correlation", Z. Ver. Deutsch. Ing., Vol. 77, p.318.

[26] Cokljat, D., Ivanov, V.A., Sarasola, F.J. and Vasquez, S.A., 2000, "Multiphase k-epsilon models for unstructured meshes", ASME paper FEDSM2000-11282, Proceedings of ASME FEDSM 2000: Fluids Engineering Division Summer Meeting, Boston USA.

[27] Hinze, J.O., 1975, Turbulence, 2nd ed., McGraw-Hill Publishing Co., New York, pp.460–471, ISBN 0-07-029037-7.

[28] Simonin, C. and Viollet, P.L. (1990), 'Predictions of an oxygen droplet pulverization in a compressible subsonic coflowing hydrogen flow', Numerical Methods for Multiphase Flows, FED-Vol. 91, pp.65–82.

[29] Cokljat, D., Slack, M., Vasquez, S.A., Bakker, A., Montante, G., 2006, "Reynolds-Stress Model for Eulerian multiphase", Progress in Computational Fluid Dynamics, An International Journal - Vol. 6, No.1/2/3 pp. 168 – 178.

[30] Mathur, S.R. and Murthy, J.Y., 1997, "A pressure based method for unstructured meshes", Numerical Heat Transfer, 31, 195–216.

[31] Kim, S.E., Mathur, S.R., Murthy, J.Y. and Choudhury, D., 1998, "A Reynolds-Averaged Navier-Stokes Solver Using Unstructured Mesh-Based Finite-Volume Scheme", AIAA Paper 98-0231.

[32] Kim, S.E., 2001, "Unstructured Mesh Based Reynolds Stress Transport Modeling of Complex Turbulent Shear Flows", AIAA Paper 2001-0728.